Stability and α decay of translead isomers and the related preformation probability of α particles

W. M. Seif* and A. R. Abdulghany
Cairo University, Faculty of Science, Department of Physics, 12613 Giza, Egypt

(Received 24 June 2023; accepted 28 July 2023; published 14 August 2023)

Nuclear isomers provide an opportunity to investigate the role of the single-particle configuration and its exotic rearrangements in nuclear stability, away from the shell closures. We explored the configurations of translead isomers from Pb to U and their stability relative to ground states, and then we investigated their well-defined α-decay modes relative to the ground-state decays. The α-preformation probability S_α is deduced from the experimental half-life and that calculated without implementing S_α, within the preformed cluster model based on the Wentzel–Kramers–Brillouin tunneling penetrability and assault frequency in terms of the Skyrme α + core potential. We found that the single valence $Z = 83, 85, 87$ protons ($\pi 1h^{1,3,5}{}_{9/2^-}$) and $N = 127$ neutron ($\nu 2g^{1}{}_{9/2^+}$) outside the doubly magic Pb core play a main role in enhancing the stability of translead isomers, whether they last in the original orbital or promote to another one, solely or coupled to another valence nucleon. The spin-gap isomers of high spin may be attributed to coupling of two protons or neutrons to stretched large spin, and then they jointly couple with a single valence nucleon. For favored α decays, the isomers indicate larger α-preformation probability than ground states. The decays from isomeric states of lower energy to higher daughter states and that involve a change in parity exhibit not only less S_α but also less relative stability than the higher-to-lower decays and those keep the parity unchanged, respectively. Increasing the difference in spin of the isomer relative to its daughter nucleus is found to enhance its stability, yielding larger half-live and smaller preformation probability.

DOI: 10.1103/PhysRevC.108.024308

I. INTRODUCTION

The α-decay process serves as a powerful tool for investigating the properties of finite nuclei in various regions of the nuclear chart. Through the study of α-particle emissions, valuable insights into nuclear structure, decay modes, and related phenomena can be obtained [1–10]. In particular, the examination of α-decay observables contributes to refining our understanding of diverse nuclear structure properties, including nuclear density distributions, static deformations, radii, proton and neutron skins, pairing and shell effects, as well as spin-parity configurations of nuclei in both their ground and excited states [11–14]. Additionally, α decay provides valuable information on the nuclear equation of state, including quantities such as the symmetry energy and incompressibility, and their isospin asymmetry dependence [15–18].

In the quest for a deeper understanding of nuclear structure and decays, the investigation of the excited and isomeric states plays a significant role. Nuclear isomers are long-lived excited states of nuclides that offer unique opportunities to explore specific nuclear phenomena and their underlying physics. The study of isomers in nuclear physics has a rich history. The concept of long-lived or stable states of a single nuclide was proposed by Soddy in 1917 [19], and in 1921 Hahn discovered the first example of an isomer [20]. Since then, extensive research has been conducted to understand the properties, formation mechanisms, and potential applications of isomers in various scientific fields [21–26]. These exotic states exhibit extended half-lives ranging from nanoseconds to years, providing valuable insights into the behavior of individual nucleons and the collective behavior of the nucleus as a whole. The latest version of the NUBASE evaluation lists data for 3340 nuclide, of which 1938 have at least one isomer with a half-life of 100 ns or longer [27], while "Atlas of Nuclear Isomers" presents data for about 2623 isomers with a half-life of 10 ns or longer [28]. Isomers have significant implications in various scientific disciplines, including astrophysics, atomic-nuclear interface studies, and the potential development of a γ-ray laser [23,28–33]. The coupling between the α-decay phenomena and isomerism provides a good opportunity to investigate the mutual transitions involving ground and excited states, as well as isomeric states [34–36].

Understanding the properties and characteristics of excited states of nuclides is crucial to unravel the mysteries of isomerism. Excited states are characterized by different arrangements of nucleons, resulting in a diverse array of isomers. Low-energy excited states typically deexcite rapidly to the ground state through electromagnetic decay, primarily via γ-ray or conversion-electron emission, within picoseconds. However, isomers represent excited states that possess extended half-lives, often due to specific factors such as spin, nuclear symmetry, or shape changes [30,37]. The existence of isomers is influenced by the interplay of individual nucleon orbits and the collective behavior of the nucleus. Spin isomers, which arise from large spin changes and low transition energies, are prevalent in low-energy states of nuclides with odd-A, with one unpaired nucleon, and odd-odd, with two

*wseif@sci.cu.edu.eg

unpaired proton and neutron, configurations [38,39]. Higher excitation energies can generate substantial spin values due to broken pairs of nucleons [40]. Another form of isomerism is associated with changes in the nuclear symmetry axis, giving rise to K isomers. Nuclei can exhibit nonspherical shapes with axial symmetry, and the projection of the total angular momentum on the symmetry axis is denoted as the K quantum number. Incomplete conservation of K allows for K-forbidden transitions, which are inhibited rather than strictly forbidden. The inhibition of decay transitions in K isomers is attributed to associated shape changes and configuration changes in individual nucleon orbits [40–43].

Shape isomers constitute a distinct class of isomers, including fission isomers and other shape-changing phenomena. Fission isomers, which have been observed in specific nuclides within certain nucleon number ranges, exhibit extended half-lives compared with the ground state [44]. These isomers are characterized by significant shape changes in the atomic nucleus and accompanying configuration changes in the individual nucleon orbits [45]. The study of shape isomers, particularly fission isomers, provides valuable insights into the behavior of atomic nuclei under extreme conditions and contributes to our understanding of nuclear structure and shape-changing phenomena [30,46].

In this context, the focus of this study is on the translead isomers and the influence of the single-particle shell structure on their stability. To provide a comprehensive analysis, we investigate the different α-decay modes of these isomers and the related α-preformation probability inside them. By examining the preformation probabilities of α particles within translead isomers, we seek to shed light on their unique characteristics and contribute to our understanding of the nuclear structure in this region. To achieve our objectives, we employ a rigorous calculation methodology based on realistic α + core interaction potentials, taking into consideration the deformation of daughter nuclei. The α-decay spectra are analyzed using precise data and semimicroscopic theoretical scheme, allowing for a quantitative evaluation of the α-particle preformation probabilities within translead isomers. Through this comprehensive analysis, we aim to contribute to the understanding of the nuclear structure and decay patterns in this particular region of the nuclear chart that provides rich structure information.

The remainder of this paper is organized as follows: In the subsequent section, we provide a detailed description of the methodology used to calculate the α-decay widths and half-lives, and to estimate the α preformation probabilities from experimental half-lives. Section III presents the analysis and discussion of the relative stability of translead isomers and their α-decay properties, comparing them to the decay modes from ground states. Finally, we conclude the paper with a summary of the main findings and their implications in Sec. IV.

II. THEORETICAL FRAMEWORK

The preformed cluster model (PCM) [47–49] will be adopted in the present study to describe the α-decay process. In the different versions of this model, the emitted α particle and the daughter nucleus are assumed to be formed as separate entities inside the parent nucleus, with a certain preformation probability S_α. Subsequently, the emitted α particle attempts to tunnel through the confining Coulomb barrier that holds the two formed fragments inside the parent nucleus. The tunneling process is significantly influenced by the shape and deformations of the daughter nucleus and its relative orientation with respect to the emitted alpha particle. The α + daughter potential can be calculated in the framework of energy density functional as the difference between the energy of the α + daughter compound system and the sum of free nuclei energy, in addition to the centrifugal potential contribution [17,50],

$$V_T(R,\theta) = \int [\mathcal{H}(\rho_\alpha(r) + \rho_D(R,r,\theta)) - \mathcal{H}(\rho_\alpha(r)) - \mathcal{H}(\rho_D(r))]dr + \frac{\hbar^2 l(l+1)}{2\mu R^2}, \quad (1)$$

where R is the separation distance between the α particle and the daughter centers. θ defines the orientation of the emitted α particle relative to the symmetry axis of the deformed daughter. l is the angular momentum carried by the emitted α particle, while μ is the reduced mass of the α + daughter system. ρ_α and ρ_D denote the densities of the α particle and daughter nuclei, respectively. The macroscopic energy density $\mathcal{H}$ includes the kinetic, nuclear, and Coulomb contributions of energy densities defined as follows:

$$\mathcal{H}(\boldsymbol{r}) = \frac{\hbar^2}{2m}[\tau_p(\boldsymbol{r}) + \tau_n(\boldsymbol{r})] + \mathcal{H}_N(\boldsymbol{r}) + \mathcal{H}_{\rm Coul}(\boldsymbol{r}), \quad (2)$$

where $\tau_{i=p,n}(\boldsymbol{r})$ are the kinetic energy densities of protons and neutrons, $\mathcal{H}_N(\boldsymbol{r})$ is the nuclear energy density, and $\mathcal{H}_{\rm Coul}(\boldsymbol{r})$ is the Coulomb energy density. The Coulomb energy density is computed based on the direct and exchange parts [51–53], and the nuclear energy density is considered in the form of Skyrme nucleon-nucleon interaction with SLy4 parametrization [54].

The proton (ρ_p) and neutron (ρ_n) density distributions of the axially symmetric deformed nucleus are expressed in the two-parameter Fermi shape,

$$\rho_i(r,\theta) = \frac{\rho_{0i}}{1+\exp\left(\frac{r-R_i(\theta)}{a_i}\right)},$$
$$R_i(\theta) = R_{0i}\left[1 + \sum_{k=2,3,4,6} \beta_k Y_k^0(\theta)\right], \quad i = p,n. \quad (3)$$

The radius R_{0i} and diffuseness a_i parameters represent the set of radial distribution parameters, while β_k represent the angular parameters of the distribution, which together determine the size and shape of the deformed distribution. The full quadrupole ($k=2$), octupole ($k=3$), hexadecapole ($k=4$), and hexacontatetrapole ($k=6$) deformations [55] are considered to account for accurate nuclear shapes. ρ_{0i} in Eq. (3) defines the central density of the distribution, calculated by normalization to the total number of particles. The deformation parameters are obtained from the FRDM(2012) mass table [55].

The kinetic ($\tau_{i=p,n}$) and radial density [$\rho_i(r)$] distributions of protons and neutrons of the involved α and daughter nuclei have been obtained by the self-consistent Hartree-Fock (HF) calculations based on the Skyrme-SLy4 NN interaction, by the sum over the included single-particle states, adding the pairing and shell corrections to the kinetic, nuclear, and Coulomb terms in Eq. (2) [56,57]:

$$\begin{aligned}\tau_i(r) &= \sum_{\beta_i} \left|\nabla\varphi_i^{\ell}(\vec{r},\sigma)\right|^2 n_{\beta_i},\\ \rho_{i=p(n)}(r) &= \sum_{\beta_i} \left|\varphi_i^{\ell}(\vec{r},\sigma)\right|^2 n_{\beta_i}.\end{aligned} \tag{4}$$

Here, $\varphi_i^{\ell}(\vec{r},\sigma)$ and n_{β_i} represent the single-particle wave functions and the corresponding occupation numbers, respectively, given in terms of the orbital (ℓ) and spin (σ) quantum numbers, $\beta \equiv (\ell,\sigma)$. The pairing correction is considered by the Bardeen-Cooper-Schrieffer (BCS) method, using a constant gap approximation [57]. The pairing energy functional is schematically expressed as a function of the constant pairing matrix elements (G_i) as

$$H_{\text{Pair}} = -\sum_{i=p,n} G_i \left[\sum_{\beta\in i}\sqrt{n_\beta(1-n_\beta)}\right]^2,$$

with the occupation weights are given in connection with the pairing gap (Δ_i) and the Fermi energy (ϵ_{Fi}) as

$$n_\beta = \frac{1}{2}\left[1 - \frac{\epsilon_\beta - \epsilon_{Fi}}{\sqrt{(\epsilon_\beta-\epsilon_{Fi})^2+\Delta_i^2}}\right].$$

Considering constant force of pairing, Δ_i and ϵ_{Fi} are determined simultaneously using the particle number restriction ($N_i = \sum_{\beta\in i} n_\beta$) and the gap function ($\Delta_i/G_i = \sum_{\beta\in i}\sqrt{n_\beta[1-n_\beta]}$). The pairing gap can be also parametrized by an average pairing gap $\widetilde{\Delta} = 11.2/\sqrt{A}$ MeV, which is acceptable for all known nuclei. While the occupation weight is unity for completely filled shells, it is determined for the partially filled shells by the adopted pairing scheme. The radius and diffuseness parameters of the density distributions of the different nuclei across the nuclear chart, which obtained from the self-consistent Skyrme (SLy4) HF + BCS calculations, had been expressed in the simple form [56]

$$\begin{aligned}R_{0n}(fm) &= 0.953N^{1/3} + 0.015Z + 0.774,\\ R_{0p}(fm) &= 1.322Z^{1/3} + 0.007N + 0.022,\\ a_n(fm) &= 0.072(N/Z) + 0.446,\\ a_p(fm) &= 0.071(Z/N) + 0.449.\end{aligned} \tag{5}$$

The spin J_i and parity π_i of the parent ($i = P$) and daughter ($i = D$) nuclei are crucial in the α-decay study, especially in the present study as we investigate α decay from isomeric states, which often exhibit various and high spin values. The angular momentum l carried by the α particle can takes values in the range $|J_P - J_D| \leqslant l \leqslant |J_P + J_D|$ such that the parity conservation condition is satisfied, $\pi_P = \pi_D(-1)^l$. Based on the principle of least action, the emitted α particle preferably carries the minimum allowed angular momentum, typically one of two values: $l = |J_P - J_D|$ or $l = |J_P - J_D| + 1$, according to the conservation of parity requirement [58].

The Wentzel–Kramers–Brillouin (WKB) approximation can be considered to deal with the α decay as a tunneling process [59]. The α particle is supposed to relocate from the inner pocket region, between the first two turning points $R_1(\theta)$ and $R_2(\theta)$, of the α + core interaction potential to the Coulomb barrier region, between $R_2(\theta)$ and R_3, with an assault frequency given by

$$\nu(\theta) = \left[\int_{R_1(\theta)}^{R_2(\theta)} \frac{2\mu}{\hbar k(R,\theta)} dR\right]^{-1}. \tag{6}$$

The orientation-dependent penetrability $P(\theta)$ of the α particle through the Coulomb barrier is then given by

$$P(\theta) = \exp\left[-2\int_{R_2(\theta)}^{R_3} k(R,\theta)dR\right]. \tag{7}$$

The wave number $k(R,\theta) = [2\mu|V_T(r,\theta) - Q_\alpha|/\hbar^2]^{1/2}$ is defined in terms of the reduced mass μ and the Q_α value of the decay. The turning points $R_i(\theta)$ are the solutions of the equation $V_T(R,\theta) = Q_\alpha$. The third turning point R_3 can be completely determined by the interacting total charges and the Q_α value, where it lies within the extreme outer region of the interaction potential, and thus it does not show orientation dependence [60,61]. For fission and cluster decays with emitted nuclei heavier than an α particle, and for fusion reactions as well, it is better to calculate the penetration probability in terms of the inertia tensor instead of the reduced mass, to account more precisely for the mass transfer and dynamics through the r-dependent inertia. The nuclear inertia tensor can be obtained using the microscopic cranking model [62], or by the classical Werner-Wheeler approximation in terms of the internuclear separation distance and the radius of the light fragment [63]. Adopting the distance between the two fragments as deformation coordinate, the effective mass and the reduced mass become the same at the touching point [62]. The small size of the α particle allows the correct use of the reduced mass in calculating the penetrability.

The α-decay width Γ is then mainly determined by averaging over orientation of the product of assault frequency $\nu(\theta)$ and the penetration probability $P(\theta)$,

$$\Gamma = \frac{1}{2}\int_0^{\pi} \nu(\theta)P(\theta)\sin(\theta)d\theta. \tag{8}$$

Finally, the partial half-life time (T_α) of a given nucleus against an α decay can be obtained in terms of the calculated decay width Γ and the preformation probability S_α as

$$T_\alpha = \frac{\ln 2}{S_\alpha \Gamma}. \tag{9}$$

The preformation probability of the alpha cluster inside the parent nucleus can be then estimated by comparing the calculated half-life using Eq. (9), without considering S_α, with the experimental partial half-life (T_α^{expt}),

$$S_\alpha = \frac{T_\alpha^{\text{calc}}(\text{without } S_\alpha)}{T_\alpha^{\text{expt}}}. \tag{10}$$

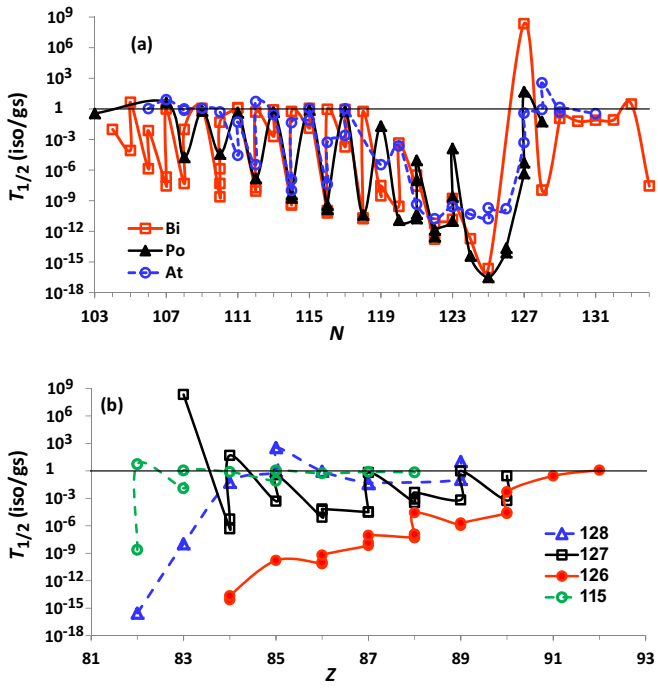

FIG. 1. The comparative half-lives $T_{1/2}(\text{iso/gs}) = T_{1/2}(\text{iso})/T_{1/2}(\text{gs})$ of the isomeric states for (a) the isotopes of Bi, Po, and At isotopes and for (b) the isotones of $N = 115$, 126, 127 and 128 relative to their ground states.

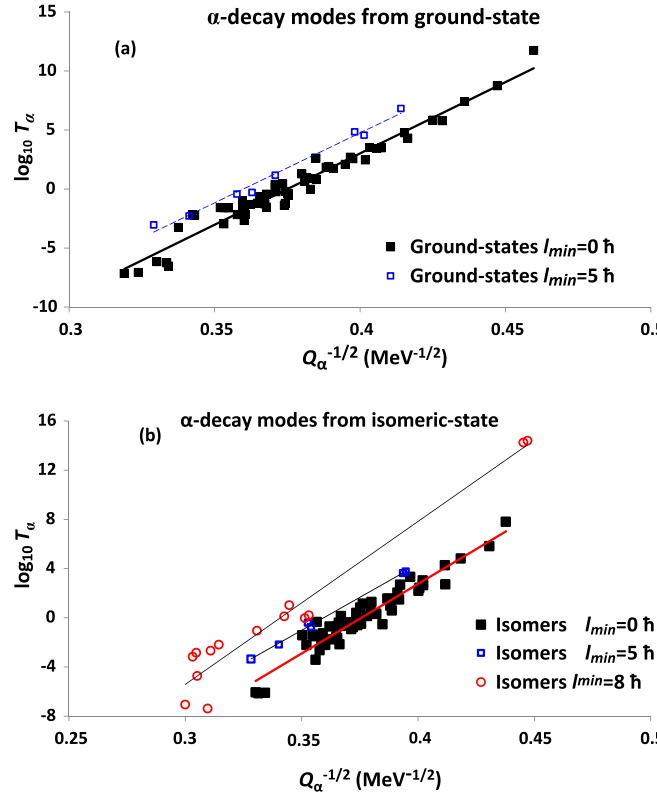

FIG. 2. The decimal logarithm of the partial half-life time ($\log_{10} T_\alpha$) for the observed favored ($l_\alpha = 0$) and unfavored [$l_{\min}(\alpha) = 5\hbar$, $8\hbar$] α-decay modes from (a) the ground states and from (b) the isomeric states of the investigated translead nuclei from Pb to U as function of $(Q_\alpha^{-1})^{1/2}$.

III. RESULTS AND DISCUSSION

A total of 292 isomers have been observed between the elements lead (Pb) and uranium (U) in the nuclear chart, spanning from ^{187}Pb ($J^\pi = 13/2^+$) to ^{239}U($5/2^+$). These isomers includes 78 even(Z)-odd(N), 77 even-even, 70 odd-odd, and 67 odd-even isomers, with relatively more participation of paired protons. Most of the observed isomers in this region of nuclear chart are those of $_{83}$Bi (57 isomers) and $_{82}$Pb (55 isomers), followed by those of $_{85}$At (36 isomers), $_{84}$Po (34 isomers), and $_{87}$Fr (32 isomers). In terms of neutron numbers, the highest number of isomers are observed in the isotones with neutron numbers $N = 126$ (24 isomers), $N = 127$ (19 isomers), and $N = 124$ (14 isomers). The most stable among these isomers are ^{210}Bi^m (9^-, $T_{1/2} = 3.04$ My), ^{204}Pb^n (9^-, 66.93 min), and ^{201}Bi^m ($1/2^+$, 57.50 min). Relative to their respective ground states (gs), the most stable isomers are ^{210}Bi^m [9^-, $T_{1/2}(\text{iso/gs}) = 2.2 \times 10^8$], ^{213}At^n ($49/2^+$, 360), and ^{211}Po^m ($49/2^+$, 48.8). The highest-spin isomeric states are observed for ^{214}Fr^p (33^+, $E = 6.675$ MeV, $T_{1/2} =$ 108 ns), ^{213}Fr^p ($65/2^-$, 8.095 MeV, 3.10 μs) and ^{211}Rn^n ($63/2^-$, 8.855 MeV, 201 ns). Furthermore, the highest-spin isomeric states observed in the most stable isomers relative to their ground states are ^{213}At^n ($49/2^+$, $E = 2.926$ MeV, $T_{1/2} = 45$ μs, $T_{1/2}(\text{iso/gs}) =$ 360), ^{217}Ac^m ($29/2^+$, 2.012 MeV, 740 ns, 10.7) and ^{211}Po^m ($25/2^+$, 1.462 MeV, 25.2 s, 48.8). It is worth noting that approximately 60% of the high-spin isomers with angular momentum $J \geqslant 17\hbar$ are observed for $N = 126 \pm 1$.

The half-lives of the observed translead isomers relative to their ground-state half-lives, $T_{1/2}(\text{iso/gs})$, are displayed for the isotopes of Bi, Po, and At in Fig. 1(a), and for the isotones of $N = 115$, 126, 127, and 128 in Fig. 1(b). While the total half-life $T_{1/2}$ reflects the overall stability of the nucleus, primarily influenced by its mass excess, pairing effects, and shell effects, $T_{1/2}(\text{iso/gs})$ will help to scrutinize the parameters that merely affect the stability of the isomeric states. Figures 1(a) and 1(b) respectively show the principle role of the single $\nu 2g^1{}_{9/2^+}$ neutron ($N = 127$) and that of the single proton $\pi 1h^1{}_{9/2^-}$ ($Z = 83$), outside the doubly magic Pb core, in enhancing the stability of the observed translead isomers. As seen in Fig. 1(a), among the identified Bi and At isomers with $T_{1/2}(\text{iso})$ greater than or equal to $T_{1/2}(\text{gs})$, there are 11 odd-N isomers and only 3 even-N isomers, and all of these are At isomers. This suggests that the presence of unpaired neutrons increases the stability of isomers with an unpaired proton. Similarly, the presence of an unpaired neutron also enhances the stability of isomers with an even number of protons. In general, among the identified isomers with $T_{1/2}(\text{iso/gs}) \geqslant 1$, there are 18 odd($Z$)-odd($N$) isomers, 8 even-odd isomers, only 4 odd-even isomers, and a single even-even isomer.

In pursuit of our main objective, the current study focuses on investigating the α-decay modes from the isomeric states of nuclei within the aforementioned translead region. A total

TABLE I. α-decay modes of translead nuclei that have $T_{1/2}$(isomer) longer than $T_{1/2}$(ground-state). The table displays the parent (Pare.) and daughter (Dau.) nuclei, the spin-parity assignment $J^{\pi}_{P(D)}$, and energy $E_{P(D)}$ (MeV) of their states involved in the decay mode, the minimum allowed value of the orbital angular momentum $l_{\min}(\hbar)$ carried out by the emitted α particle, the energy released Q_{α} (MeV) in the decay [64,65], the observed half-life time $T^{\exp}_{1/2}(s)$, the experimental intensity I_{α}% of the α-decay mode and its partial half-life time $T^{\exp}_{\alpha}(s)$ [64,66], and the ratio of $T^{\exp}_{\alpha}$ the decay modes from the isomeric state to that form the ground-state (gs). The parentheses ( ) and square brackets [ ] indicate uncertain and non-experimental spin-parity assignments, respectively [64,66]. The upper suffix m and n of the isotope indicate its first and second isomeric states [66], respectively. The last column presents the estimated preformation probability $T^{\exp}_{\alpha}(s)$ (Eq. (10)), based on the experimental $T^{\exp}_{\alpha}$ and that calculated in the present work without considering S_{α}, T^{cal}_{α} (without S_{α}). The uncertainty in both Q_{α} and $T^{\exp}_{\alpha}$ are considered to evaluate the uncertainty in $S^{\exp}_{\alpha}$.

Pare.	Dau.	J^{π}_{P}	J^{π}_{D}	$l_{\min}$ ($\hbar$)	E_P (MeV)	E_D (MeV)	Q_{α} (MeV)	$T^{exp}_{1/2}$ (s)	I_{α} (%)	T^{exp}_{α} (s)	T_{α}/T_{α}(gs)	S^{exp}_{α} (Eq. (10))
^{187}Pb	^{183}Hg	3/2$^-$	3/2$^-$	0	gs	0.0674	6.3256±0.0060	15.20±0.300	4.200	361.900±7.143		0.0049±0.0004
^{187}Pb^m		13/2$^+$	13/2$^+$	0	0.0330	0.1830	6.2430±0.0060	18.30±0.300	12.000	152.500±2.500	0.423	0.0256±0.0015
^{191}Pb	^{187}Hg	(3/2$^-$)	3/2$^{(-)}$	0	gs	gs	5.4500±0.0400	79.80±4.80	0.013	(6.138±0.369)×10^5		0.0394±0.0187
^{191}Pb^m		13/2$^{(+)}$	(13/2$^+$)	0	≈ 0	0.059	5.3910±0.0400	130.80±4.80	0.020	(6.540±0.240)×10^5	1.092	0.0789±0.0406
^{194}Bi	^{190}Tl	(3$^+$)	2$^-$	1	gs	gs	5.9180±0.0050	95.00±3.000	2.7×10^{-3}	(3.519±0.111)×10^6		0.0001±0.00001
^{194}Bi		(3$^+$)	(3$^+$)	0	gs	0.1510	5.7670±0.0050	95.00±3.000	0.460	(2.065±0.065)×10^4		0.0512±0.0041
^{194}Bi^n		(10$^-$)	(7$^+$)	3	0.184	0.0830	6.0190±0.0050	115.00±4.000	0.007	(1.643±0.057)×10^6	0.467	0.0002±0.00001
^{194}Bi^n		(10$^-$)	(10$^-$)	0	0.184	0.3890	5.7130±0.0050	115.00±4.000	0.180	(6.389±0.222)×10^4	0.018	0.0304±0.0028
^{210}Bi	^{206}Tl	1$^-$	1$^-$	0	gs	0.3049	4.7311±0.0080	(433.04±0.43)×10^3	7.9×10^{-5}	(5.481±0.005)×10^{11}		0.0006±0.0001
^{210}Bi^m		9$^-$	0$^-$	10	0.2713	gs	5.3073±0.0080	(95.90±1.89)×10^{12}	10^{-4}	(9.594±0.189)×10^{19}	1.8×10^8	(3.0±0.4)×10^{-11}
^{210}Bi^m		9$^-$	2$^-$	8	0.2713	0.2656	5.0417±0.0080	(95.90±1.89)×10^{12}	55.000	(1.744±0.034)×10^{14}	3.2×10^2	(2.5±0.3)×10^{-5}
^{210}Bi^m		9$^-$	1$^-$	8	0.2713	0.3049	5.0024±0.0080	(95.90±1.89)×10^{12}	39.500	(2.429±0.048)×10^{14}	4.4 ×10^2	(3.1±0.4)×10^{-5}
^{211}Po	^{207}Pb	9/2$^+$	1/2$^-$	5	gs	gs	7.5945±0.0005	(5.16±0.03) ×10^{-1}	98.916	0.522±0.003		0.0033±0.0001
^{211}Po^m		(25/2$^+$)	13/2$^+$	6	1.4620	1.6334	7.4231±0.0005	25.20±0.60	99.980	25.210±0.600	48.317	0.0010±0.0001
^{191}At	^{187}Bi	(1/2$^+$)	1/2$^+$	0	gs	0.1120	7.7080±0.0300	(2.10±0.80)×10^{-3}	100	(2.100±0.800)×10^{-3}		0.1543±0.0852
^{191}At^m		(7/2$^-$)	9/2$^-$	2	0.0550	gs	7.8750±0.0300	(2.20±0.40)×10^{-3}	2.000	0.110±0.020	52.381	0.0014±0.0005
^{191}At^m		(7/2$^-$)	7/2$^-$	0	0.0550	0.0630	7.8120±0.0300	(2.20±0.40)×10^{-3}	98.000	(2.245±0.408)×10^{-3}	1.069	0.0571±0.0218
^{197}At	^{193}Bi	(9/2$^-$)	(9/2$^-$)	0	gs	gs	7.1040±0.0030	(38.10±0.60) ×10^{-2}	96.100	0.397±0.006		0.0519±0.0022
^{197}At^m		(1/2$^+$)	(1/2$^+$)	0	0.0520	0.3080	6.8480±0.0030	2.00±0.20	100.000	2.000±0.200	5.045	0.0953±0.0129
^{200}At	^{196}Bi	(3$^+$)	(3$^+$)	0	gs	gs	6.5964±0.0014	43.00±1.00	57.000	75.440±1.754		0.0207±0.0008
^{200}At^m		(7$^+$)	(3$^+$)	4	0.1040	gs	6.7004±0.0014	47.00±1.00	0.360	(1.306±0.028)×10^4	173.062	0.0005±0.0001
^{200}At^m		(7$^+$)	(7$^+$)	0	0.1040	0.1670	6.5334±0.0014	47.00±1.00	43.000	109.300±2.326	1.449	0.0259±0.0008
^{200}At^n		(10$^-$)	(10$^-$)	0	0.3350	0.2690	6.6624±0.0014	3.50±0.20	10.500	33.330±1.905	0.442	0.0256±0.0020
^{214}At	^{210}Bi	(1$^-$)	1$^-$	0	gs	gs	8.9870±0.0040	(5.58±0.10)×10^{-7}	98.950	(5.639±0.101)×10^{-7}		0.0332±0.0014
^{214}At^n		(9$^-$)	9$^-$	0	0.2320	0.2712	8.9478±0.0040	(7.60±0.15)×10^{-7}	99.180	(7.663±0.151)×10^{-7}	1.359	0.0307±0.0014
^{200}Fr	^{196}At	(3$^+$)	(3$^+$)	0	gs	gs	7.6210±0.0500	(4.90±0.40) ×10^{-2}	100	0.049±0.004		0.1163±0.0521
^{200}Fr^m		[10$^-$]	(10$^-$)	0	0.0500	0.0400	7.6310±0.0500	0.19±0.12	100	0.190±0.120	3.878	0.0546±0.0444

TABLE I. *(Continued).*

Pare.	Dau.	J_P^π	J_D^π	$l_{\min}$ ($\hbar$)	E_P (MeV)	E_D (MeV)	Q_α (MeV)	$T_{1/2}^{exp}$ (s)	I_α (%)	T_α^{exp} (s)	T_α/T_α(gs)	S_α^{exp} (Eq. (10))
^{204}Fr	^{200}At	3^+	(3^+)	0	gs	gs	7.1713±0.0025	1.90±0.50	70.000	2.714±0.714		0.0389±0.0110
^{204}Fr^m		(7^+)	(3^+)	4	0.0470	gs	7.2183±0.0025	2.00±0.10	0.210	(9.524±0.476)×10^2	3.5×10^2	0.0005±0.0001
^{204}Fr^m		(7^+)	(7^+)	0	0.0470	0.1130	7.1053±0.0025	2.00±0.10	30.000	6.667±0.333	2.456	0.0260±0.0018
^{204}Fr^n		(10^-)	(10^-)	0	0.3160	0.3440	7.1433±0.0025	0.80±0.20	100	0.800±0.200	0.295	0.1698±0.0494
^{206}Fr	^{202}At	$(2^+,3^+)$	$(2^+,3^+)$	0	gs	gs	6.9230±0.0040	16.00	84.000	19.050		0.0346±0.0015
^{206}Fr^m		$7^{(+)}$	(7^+)	0	≈ 0	≈ 0	6.9230±0.0040	16.00	84.000	19.050	1.000	0.0346±0.0015
^{206}Fr^n		$10^{(-)}$	(10^-)	0	0.5310	0.3920	7.0620±0.0040	0.70±0.10	5.000	14.000±2.000	0.735	0.0147±0.0023
^{216}Fr	^{212}At	(1^-)	(1^-)	0	gs	gs	9.1740±0.0030	(7.00±0.20)×10^{-7}	99.000	(7.071±0.202)×10^{-7}		0.0454±0.0022
^{216}Fr^n		(3^-)	(3^-)	0	0.1333	0.2053	9.1020±0.0030	(7.10±0.50)×10^{-8}	10.000	(7.100±0.500)×10^{-7}	1.004	0.0687±0.0062
^{216}Fr^m		(9^-)	(9^-)	0	0.2190	0.2229	9.1701±0.0030	(8.50±0.30)×10^{-7}	100.000	(8.500±0.300)×10^{-7}	1.202	0.0385±0.0021
^{218}Fr	^{214}At	(1^-)	1^-	0	gs	gs	8.0137±0.0014	(1.000±0.600)×10^{-3}	92.000	(1.087±0.652)×10^{-3}		0.0648±0.0393
^{218}Fr		(1^-)	$(2)^-$	2	gs	0.1451	7.8686±0.0014	(1.000±0.600)×10^{-3}	1.500	(6.667±4.000)×10^{-2}		0.0055±0.0033
^{218}Fr		(1^-)	$(1^-,2^-)$	0	gs	0.3040	7.7097±0.0014	(1.000±0.600)×10^{-3}	5.000	(2.000±1.200)×10^{-2}		0.0323±0.0196
^{218}Fr^m		$(8^-,9^-)$	1^-	8	0.0860	gs	8.0997±0.0014	(2.190±0.050)×10^{-2}	2.400	0.913±0.021	839.500	0.0060±0.0002
^{218}Fr^m		$(8^-,9^-)$	(8^-)	0	0.0860	0.3430	7.7567±0.0014	(2.190±0.050)×10^{-2}	41.300	0.053±0.001	48.785	0.0055±0.0002
^{218}Fr^m		$(8^-,9^-)$	(7^-)	2	0.0860	0.2779	7.8218±0.0014	(2.190±0.050)×10^{-2}	15.900	0.138±0.003	126.717	0.0024±0.0001
^{218}Fr^m		$(8^-,9^-)$	9^-	0	0.0860	0.2310	7.8687±0.0014	(2.190±0.050)×10^{-2}	4.800	0.456±0.010	419.750	0.0003±0.00001
^{218}Fr^m		$(8^-,9^-)$	(6^-)	2	0.0860	0.3021	7.7976±0.0014	(2.190±0.050)×10^{-2}	10.900	0.201±0.005	184.844	0.0020±0.0001
^{218}Fr^m		$(8^-,9^-)$	$(8^-)_2$	0	0.0860	0.7284	7.3713±0.0014	(2.190±0.050)×10^{-2}	9.500	0.231±0.005	212.084	0.0251±0.0008
^{218}Fr^m		$(8^-,9^-)$	(0^-)	8	0.0860	0.0790	8.0207±0.0014	(2.190±0.050)×10^{-2}	1.400	1.564±0.036	1439.143	0.0285±0.0009
^{218}Fr^m		$(8^-,9^-)$	$(2)^-$	6	0.0860	0.1451	7.9546±0.0014	(2.190±0.050)×10^{-2}	1.600	1.369±0.031	1259.250	0.0041±0.0002
^{218}Fr^m		$(8^-,9^-)$	(3^-)	6	0.0860	0.1870	7.9127±0.0014	(2.190±0.050)×10^{-2}	1.140	1.921±0.044	1767.368	0.0039±0.0002
^{206}Ac	^{202}Fr	(3^+)	(3^+)	0	gs	gs	7.9450±0.0500	(2.50±0.70)×10^{-2}	100	0.025±0.007		0.0526±0.0304
^{206}Ac^m		(10^-)	(10^-)	0	≈ 0	≈ 0	7.9450±0.0500	(4.10±1.60)×10^{-2}	100	0.041±0.016	1.640	0.0361±0.0236
^{216}Ac	^{212}Fr	(1^-)	5^+	5	gs	gs	9.2350±0.0060	(4.40±0.16)×10^{-4}	47.500	(9.263±0.337)×10^{-4}		0.0029±0.0002
^{216}Ac		(1^-)	(4^+)	3	gs	0.0825	9.1525±0.0060	(4.40±0.16)×10^{-4}	48.800	(9.016±0.328)×10^{-4}		0.0008±0.0001
^{216}Ac^m		(9^-)	5^+	5	0.048	gs	9.2830±0.0060	(4.41±0.07)×10^{-4}	100	(4.410±0.070)×10^{-4}	0.476	0.0046±0.0002
^{217}Ac	^{213}Fr	$9/2^-$	$9/2^-$	0	gs	gs	9.8320±0.0100	(6.90±0.40)×10^{-8}	100	(6.900±0.400)×10^{-8}		0.0701±0.0077
^{217}Ac^m		$(29/2^+)$	$9/2^-$	11	2.0122	gs	11.8442±0.0100	(7.40±0.40)×10^{-7}	0.122	(6.066±0.328)×10^{-4}	8790.687	(5.0±0.6)×10^{-5}
^{217}Ac^m		$(29/2^+)$	$(13/2)^+$	8	2.0122	1.1050	10.7392±0.0100	(7.40±0.40)×10^{-7}	4.100	(1.805±0.098)×10^{-5}	261.577	0.0018±0.0013
^{217}Ac^m		$(29/2^+)$	$7/2^-$	11	2.0122	0.4900	11.3542±0.0100	(7.40±0.40)×10^{-7}	0.320	(2.313±0.125)×10^{-4}	3351.449	0.0002±0.0001
^{217}Ac^n		$19/2^-$	$9/2^-$	6	1.4981	gs	11.3301±0.0100	(8.00±2.00)×10^{-9}	0.590	(1.356±0.339)×10^{-6}	19.651	(5.9±1.7)×10^{-5}
^{218}U	^{214}Th	0^+	0^+	0	gs	gs	8.7750±0.0090	(5.50±1.40)×10^{-4}	100	(5.500±1.400)×10^{-4}		0.0618±0.0194
^{218}U^m		(8^+)	0^+	8	2.1050	gs	10.880±0.0090	(6.60±2.00)×10^{-4}	100	(6.600±2.000)×10^{-4}	1.200	0.0003±0.0001

of 105 α-decay modes from 70 isomers of 62 nuclei, ranging from $^{187}_{82}Pb_{105}$ to $^{218}_{92}U_{126}$, will be compared with their corresponding 81 decays from ground states. These represent the well-defined α-decay modes observed from the aforementioned isomers [64,65]. Figures 2(a) and 2(b) show the partial half-life time against α decay for the decay modes from ground states and from isomeric states, respectively, as functions of $(Q_\alpha^{-1})^{1/2}$, for all decay modes under study. For these decays, the minimum allowed orbital angular momentum ($l_{\min}$) transferred by the emitted α particle, to conserve the angular momentum and parity, is $0\hbar$ for the favored decays from 58 ground states and 60 isomeric states. According to the spin-parity assignments of the parent and daughter states involved in each decay mode, $l_{\min}$ reaches $5\hbar$ for the decays from the ground states of ^{189,193,195}Bi ($J^\pi = 9/2^-$), ^{212}Bi(1^-), ^{211}Po($9/2^+$), ^{212}At(1^-), ^{214}Fr(1^-), and ^{216}Ac(1^-). For decays from isomeric states, $l_{\min}$ reaches $11\hbar$ for the decays from ^{217}Ac^m($29/2^+$) to ^{213}Fr($9/2^-$ and $7/2^-$). As seen in Fig. 2, the observed $\log_{10} T_\alpha$ for the decay modes from both the ground states [Fig. 2(a)] and isomeric states [Fig. 2(b)] tend to increase linearly with $(Q_\alpha^{-1})^{1/2}$, with distinctive characteristic lines corresponding to different values of $l_{\min}$. Such characteristic lines can be employed to estimate the unknown spin-parity assignment of a given nuclear state based on its observed half-life time. In general, the half-life times tend to increase as the transferred angular momentum increases.

Twenty-one of the investigated translead nuclei, which possess well-defined α-decay modes, exhibit longer-lived isomers compared with their ground states. The α-decay modes of these nuclei, from their ground and isomeric states, are presented in Table I. The first seven columns of Table I respectively identify the parent P and daughter D nuclei, the spin and parity J^π of the states involved in the decay process, the minimum allowed value of the orbital angular momentum transferred by the emitted α particle ($l_{\min}$) for angular-momentum conservation, and the energy of the involved states. Different isomers of the same nucleus are distinguished by the upper suffixes m and n [66]. The released energy Q_α (MeV) [64,65] in the decay is presented in column 8, taking into account the energy of the involved states. The total half-life time $T_{1/2}^{\text{expt}}$ (s) of the nucleus and of its isomer(s), the intensity $I_\alpha(\%)$ of the decay mode [64,66] and its corresponding partial half-life time T_α^{expt} are listed in columns 9–11, respectively. Column 12 displays the ratio of the partial T_α^{expt} of the isomeric decay mode to its corresponding T_α^{expt}(gs). The deduced preformation probabilities S_α^{expt} that are listed in the last column, are obtained using Eq. (10) in terms of the experimental partial half-life time and that calculated in the present work [Eq. (9)] without considering S_α. The uncertainties in Q_α that are used to calculate T_α, and in T_α^{expt}, are taken into account in determining the uncertainty of the estimated values of S_α. The details of the α-decay modes for the investigated isomers that exhibit slightly shorter half-lives compared with their ground states [$0.1 \leqslant T_{1/2}(\text{iso/gs}) < 1$] are listed in Table II. Table III presents information and calculations related to the α decays of the significantly less stable isomers under study, with $T_{1/2}(\text{iso/gs}) < 0.1$.

The most stable known isomers are ^{180}Ta^m($J^\pi = 9^-$, $T_{1/2} > 7.15\ Py$) in the transtin region and the translead ^{210}Bi^m(9^-, $T_{1/2} = 3.04$ My), which have significantly longer half-lives compared with their respective ground-state nuclei, ^{180}Ta(1^+, 8.154 h) and ^{210}Bi(1^-, 5.012 d) [64]. ^{210}Bi possesses a single valence proton ($\pi 1h^1{}_{9/2^-}$) and single valence neutron ($\nu 2g^1{}_{9/2^+}$) outside a doubly magic ^{208}Pb core. With this ($\pi 1h^1{}_{9/2^-} \bigotimes \nu 2g^1{}_{9/2^+}$) configuration for this nucleus, the 1^- ground state is observed, instead of the expected 0^- state that appeared next to it with $E = 46.059$ keV and $T_{1/2} < 3$ ns [64]. The long-lived 9^- (271.31 keV) isomeric state is observed as the third energy level of ^{210}Bi. Similar coupling between the single valence proton ($\pi 1h^1{}_{9/2^-}$) and a valence unpaired neutron is also observed in relatively more stable isomers such as ^{188}Bi^m [10^- ($\pi 1h^1{}_{9/2^-} \bigotimes \nu 1i^5{}_{13/2^+}$), $T_{1/2}(\text{iso/gs}) = 4.417$], ^{216}Bi^m [$3^-$ ($\pi 1h^1{}_{9/2^-} \bigotimes \nu 2g^7{}_{9/2^+}$), 2.933], ^{194}Bi^m [$6^+$, 7^+ ($\pi 1h^1{}_{9/2^-} \bigotimes \nu 1i^{11}{}_{13/2^+}$), 1.316], ^{194}Bi^n [$10^-$ ($\pi 1h^1{}_{9/2^-} \bigotimes \nu 1i^{11}{}_{13/2^+}$), 1.211], ^{192}Bi^m [$10^-$ ($\pi 1h^1{}_{9/2^-} \bigotimes \nu 1i^9{}_{13/2+}$), 1.145], and ^{198}Bi^m [7^+ ($\pi 1h^1{}_{9/2^-} \bigotimes \nu 3p^1{}_{3/2^+}$), 1.127], and in the relatively less stable isomers such as ^{190}Bi^m [10^- ($\pi 1h^1{}_{9/2^-} \bigotimes \nu 1i^7{}_{13/2^+}$), 0.984], ^{200}Bi^m [$2^+$ ($\pi 1h^1{}_{9/2^-} \bigotimes \nu 3p^3{}_{3/2^+}$), 0.852], ^{196}Bi^n [$10^-$ ($\pi 1h^1{}_{9/2^-} \bigotimes \nu 1i^{13}{}_{13/2^+}$), 0.780], and ^{212}Bi^m [9^- ($\pi 1h^1{}_{9/2^-} \bigotimes \nu 2g^3{}_{9/2^+}$), 0.413]. Additionally, there are fifteen observed (odd-N) Bi isomers with $10^{-11} < T_{1/2}(\text{iso/gs}) < 0.2$. Regarding the Bi isomers with paired neutrons, 31 (even-N) Bi isomers have been observed, among which are the relatively more stable ^{195,197,199,201}Bi^m [$1/2^+$, $T_{1/2}(\text{iso/gs}) \geqslant 0.5$], ^{187,189,191,193}Bi^m [$1/2^+$, $0.001 \leqslant T_{1/2}(\text{iso/gs}) \leqslant 0.05$], ^{215}Bi^m ($25/2^-$, 0.08), and ^{213}Bi^m ($25/2^-$, 0.06) isomers. The occurrence of the $1/2^+$ state in ten Bi isomers suggests a possible ($\pi 1h^2{}_{9/2^-} \bigotimes 3s^{-1}{}_{1/2^+}$) proton configuration, where a proton pair in the $\pi 3s_{1/2^+}$ state may be split, with the promotion of one of the protons to occupy a vacancy in the $\pi 1h_{9/2^-}$ orbital, leaving an excited $3s_{1/2^+}$ state with a hole. Such a scenario has been suggested to explain certain nuclear ground states [67].

In addition to the isomer ^{210}Bi^m, the role of a single valence neutron ($\nu 2g^1{}_{9/2^+}$) outside the closed shell $N = 126$ is also evident in the relatively more stable isomer ^{211}Po^m [$25/2^+$ ($\pi 1h^2{}_{9/2^-} \bigotimes \nu 2g^1{}_{9/2^+}$), $T_{1/2}(\text{iso/gs}) = 48.837$] compared with its ground state. The high spin value of $25/2^+$ can be attributed to the ($\pi 1h^2{}_{9/2^-} \bigotimes \nu 2g^1{}_{9/2^+}$) configuration, via stretching the protons pair in the $\pi 1h^2{}_{9/2^-}$ orbital to have spin $8\hbar$. This is analogous to the high spin state of ^{211}Bi^m($25/2^-$), which occurs with ($\pi 1h^1{}_{9/2^-} \bigotimes \nu 2g^2{}_{9/2^+}$) configuration [68]. In addition to α decay, the high-spin state of the spin-gap isomer ^{211}Po^m ($25/2^+, E = 1.462$ MeV) can decay to lower observed states of $17/2^+$ ($E = 1.428$ MeV), $15/2^+$ (1.459 MeV), or $15/2^-$ (1.065 MeV) states through $E4$, $M5$, or $E5$ γ transitions, respectively. The lower $23/2^+$, $21/2^+$, and $19/2^+$ states, which could be more readily connected to the $15/2^+$ state via $M1$, $E2$, or $M3$ transitions, are not observed in ^{211}Po. That is why ^{211}Po^m ($25/2^+$) is classified as a spin-gap isomer that does not exhibit γ transitions of low spin change [69]. Furthermore, the same neutron state ($\nu 2g^1{}_{9/2^+}$) is coupled with the unpaired $\pi 1h_{9/2^-}$ proton, resulting in the formation of isomers

TABLE II. Same as Table I, but for the translead nuclei that have isomers of less, but comparable, half-lives relative to their ground-state decays, $1 > T_{1/2}(\text{isomer})/T_{1/2}(\text{gs}) \geqslant 0.1$.

Pare.	Dau.	J_P^π	J_D^π	$l_{\min}$ ($\hbar$)	E_P (MeV)	E_D (MeV)	Q_α (MeV)	$T_{1/2}^{exp}$ (s)	I_α (%)	T_α^{exp} (s)	T_α/T_α^{min}(gs)	S_α^{exp} (Eq. (10))
^{190}Bi	^{186}Tl	(3^+)	(2^-)	1	Gs	gs	6.8620±0.0030	6.300±0.100	77.000	8.182±0.130		0.0042±0.0002
^{190}Bi^m		(10^-)	(10^-)	0	0.191	0.414	6.6390±0.0030	6.200±0.100	67.000	9.254±0.149	1.131	0.0212±0.0011
^{196}Bi	^{192}Tl	(3^+)	(3^+)	0	Gs	0.178	5.2600±0.0400	307.800±12.100	1.2×10^{-3}	$(2.565\pm0.100)\times10^7$		0.0196±0.0099
^{196}Bi^n		(10^-)	(10^-)	0	0.271	0.491	5.2180±0.0400	240.000±3.000	3.8×10^{-4}	$(6.316\pm0.079)\times10^7$	2.530	0.0135±0.0066
^{212}Bi	^{208}Tl	$1^{(-)}$	5^+	5	gs	gs	6.2070±0.0030	$(36.330\pm0.036)\times10^2$	9.750	$(3.726\pm0.004)\times10^4$		0.0026±0.0001
^{212}Bi		$1^{(-)}$	4^+	3	gs	0.0399	6.1670±0.0030	$(36.330\pm0.036)\times10^2$	25.130	$(1.446\pm0.001)\times10^4$		0.0013±0.00004
^{212}Bi^m		(9^-)	5^+	5	0.2500	gs	6.4570±0.0030	$(15.000\pm0.012)\times10^2$	35.000	$(4.286\pm0.034)\times10^3$	0.115	0.0019±0.0001
^{212}Bi^m		(9^-)	4^+	5	0.2500	0.0399	6.4170±0.0030	$(15.000\pm0.012)\times10^2$	26.000	$(5.769\pm0.046)\times10^3$	0.155	0.0021±0.0001
^{193}Po	^{189}Pb	$(3/2^-)$	$(3/2^-)$	0	gs	gs	7.0940±0.0040	0.388±0.040	99.300	0.391±0.040		0.0266±0.0036
^{193}Po		$(3/2^-)$	$(3/2^-)_2$	0	gs	0.5490	6.5450±0.0040	0.388±0.040	0.700	55.430±5.714		0.0237±0.0033
^{193}Po^m		$(13/2^+)$	$(13/2^+)$	0	0.0950	0.0400	7.1490±0.0040	0.245±0.011	99.200	0.247±0.011	0.632	0.0265±0.0021
^{193}Po^m		$(13/2^+)$	$(13/2^+)_2$	0	0.0950	0.6770	6.5120±0.0040	0.245±0.011	0.800	30.630±1.375	78.378	0.0581±0.0048
^{195}Po	^{191}Pb	$(3/2^-)$	$(3/2^-)$	0	gs	gs	6.7460±0.0030	4.640±0.090	75.000	6.187±0.120		0.0313±0.0018
^{195}Po		$(3/2^-)$	$(3/2^-)_2$	0	gs	0.5970	6.1490±0.0030	4.640±0.090	0.140	$(3.314\pm0.064)\times10^3$		0.0182±0.0010
^{195}Po^m		$(13/2^+)$	$(13/2^+)$	0	0.1100	≈ 0	6.8560±0.0030	1.920±0.020	90.000	2.133±0.022	0.345	0.0340±0.0011
^{195}Po^m		$(13/2^+)$	$(13/2^+)_2$	0	0.1100	0.6700	6.1860±0.0030	1.920±0.020	0.180	$(1.067\pm0.011)\times10^3$	172.414	0.0390±0.0012
^{197}Po	^{193}Pb	$(3/2^-)$	$(3/2^-)$	0	gs	gs	6.4120±0.0030	53.600±1.000	44.000	121.800±2.273		0.0313±0.0012
^{197}Po^m		$(13/2^+)$	$13/2^+$	0	0.2040	≈ 0	6.6160±0.0030	25.800±0.100	84.000	30.710±0.119	0.252	0.0180±0.0005
^{199}Po	^{195}Pb	$3/2^-$	$(3/2^-)$	0	gs	gs	6.0740±0.0019	328.200±9.000	12.000	$(2.735\pm0.075)\times10^3$		0.0403±0.0019
^{199}Po^m		$(13/2^+)$	$13/2^{(+)}$	0	0.3100	0.2010	6.1830±0.0019	250.200±3.000	39.000	$(6.415\pm7.692)\times10^2$	0.235	0.0507±0.0016
^{201}Po	^{197}Pb	$3/2^-$	$3/2^-$	0	gs	gs	5.7990±0.0017	918.000±12.000	1.600	$(5.738\pm0.075)\times10^4$		0.0322±0.0010
^{201}Po^m		$13/2^+$	$13/2^+$	0	0.4240	0.3193	5.9040±0.0017	534.000±12.000	2.9000	$(1.841\pm0.041)\times10^4$	0.321	0.0308±0.0012
^{212}Po	^{208}Pb	0^+	0^+	0	gs	gs	8.9541±0.0001	$(2.990\pm0.020)\times10^{-7}$	100	$(2.990\pm0.020)\times10^{-7}$		0.0317±0.0002
^{212}Po^m		(8^+)	0^+	8	1.4764	gs	10.4305±0.0001	$(1.710\pm0.020)\times10^{-8}$	42.000	$(4.071\pm0.048)\times10^{-8}$	0.136	0.1285±0.0016
^{193}At	^{189}Bi	$(1/2^+)$	$(1/2^+)$	0	gs	0.1840	7.3880±0.0070	0.029±0.005	100	0.029±0.005		0.0916±0.0206
^{193}At^m		$(7/2^-)$	$(9/2^-)$	2	0.0210	gs	7.5930±0.0070	0.021±0.005	2.000	1.050±0.250	36.207	0.0010±0.0003
^{193}At^m		$(7/2^-)$	$(7/2^-)$	0	0.0210	0.1000	7.4930±0.0070	0.021±0.005	98.000	0.021±0.005	0.739	0.0566±0.0163
^{193}At^n		$(13/2^+)$	$(13/2^+)$	0	0.0390	0.3580	6.2530±0.0070	0.028±0.004	24.000	0.117±0.017	4.023	0.0664±0.0131
^{195}At	^{191}Bi	$(1/2^+)$	$(1/2^+)$	0	gs	0.2410	7.0980±0.0050	0.290±0.020	100	0.290±0.020		0.0893±0.0105
^{195}At^m		$(7/2^-)$	$(9/2^-)$	2	0.0320	gs	7.3710±0.0050	0.143±0.003	4.000	3.575±0.075	12.328	0.0015±0.0001
^{195}At^m		$(7/2^-)$	$(7/2^-)$	0	0.0320	0.1490	7.2220±0.0050	0.143±0.003	84.00	0.170±0.004	0.587	0.0538±0.0032
^{199}At	^{195}Bi	$9/2^{(-)}$	$(9/2^-)$	0	gs	gs	6.7772±0.0012	6.920±0.130	90.000	7.689±0.144		0.0407±0.0010
^{199}At^m		$1/2^+$	$1/2^+$	0	0.2400	0.4010	6.6162±0.0012	0.310±0.080	1.000	31.000±8.000	4.032	0.0493±0.0138

TABLE II. *(Continued).*

Pare.	Dau.	J_P^π	J_D^π	$l_{\min}$ ($\hbar$)	E_P (MeV)	E_D (MeV)	Q_α (MeV)	$T_{1/2}^{exp}$ (s)	I_α (%)	T_α^{exp} (s)	T_α/T_α^{min}(gs)	S_α^{exp} (Eq. (10))
^{198}At	^{194}Bi	(3^+)	(3^+)	0	gs	gs	6.8894±0.0019	4.460±0.100	97.000	4.598±0.103		0.0266±0.0010
^{198}At^m		(10^-)	(10^-)	0	0.2650	0.1610	6.9934±0.0019	1.250±0.060	93.000	1.344±0.065	0.292	0.0371±0.0025
^{198}At^m		(10^-)	(9^-)	2	0.2650	0.2655	6.8889±0.0019	1.250±0.060	0.180	694.400±33.330	151.034	0.0003±0.0001
^{202}At	^{198}Bi	$(2^+,3^+)$	$(2^+,3^+)$	0	gs	gs	6.3538±0.0013	184.000±1.000	37.000	$(4.973\pm0.027)\times10^2$		0.0291±0.0007
^{202}At^m		$7^{(+)}$	7^+	0	≈ 0	≈ 0	6.3538±0.0013	182.000±2.000	8.700	$(2.092\pm0.023)\times10^3$	4.207	0.0069±0.0002
^{202}At^n		$10^{(-)}$	10^-	0	0.3917	0.2490	6.4965±0.0013	0.460±0.050	0.096	479.200±52.100	0.964	0.0075±0.0009
^{212}At	^{208}Bi	(1^-)	5^+	5	gs	gs	7.8172±0.0006	0.314±0.002	83.200	0.377±0.002		0.0023±0.0001
^{212}At		(1^-)	4^+	3	gs	0.0626	7.7546±0.0006	0.314±0.002	15.400	2.039±0.013		0.0001±0.00001
^{212}At^m		(9^-)	5^+	5	0.2229	gs	8.0401±0.0006	0.119±0.003	30.700	0.388±0.010	1.027	0.0004±0.00001
^{212}At^m		(9^-)	4^+	5	0.2229	0.0629	7.9772±0.0006	0.119±0.003	67.600	0.176±0.004	0.466	0.0016±0.0001
^{195}Rn	^{191}Po	$3/2^-$	$(3/2^-)$	0	gs	gs	7.6900±0.0070	0.007±0.003	99.750	0.007±0.003		0.0485±0.0353
^{195}Rn^m		$13/2^+$	$(13/2^+)$	0	0.0590	0.0400	7.7090±0.0070	0.006±0.003	99.800	0.006±0.003	0.857	0.0420±0.0306
^{197}Rn	^{193}Po	$(3/2^-)$	$(3/2^-)$	0	gs	gs	7.4110±0.0070	0.054±0.006	100	0.054±0.006		0.0934±0.0154
^{197}Rn^m		$(13/2^+)$	$(13/2^+)$	0	0.1990	0.1000	7.5100±0.0070	$(2.560\pm0.250)\times10^{-2}$	100	$(2.560\pm0.250)\times10^{-2}$	0.474	0.0901±0.0135
^{199}Rn	^{195}Po	$(3/2^-)$	$(3/2^-)$	0	gs	gs	7.1400±0.0500	0.590±0.030	94.000	0.628±0.032		0.0929±0.0400
^{199}Rn^m		$(13/2^+)$	$(13/2^+)$	0	0.1800	0.2300	7.0900±0.0500	0.310±0.020	97.000	0.320±0.021	0.509	0.2865±0.1338
^{201}Rn	^{197}Po	$(3/2^-)$	$(3/2^-)$	0	gs	gs	6.8610±0.0500	7.100±0.800	78.000	9.103±1.026		0.0653±0.0330
^{201}Rn^m		$(13/2^+)$	$(13/2^+)$	0	0.2800	0.2040	6.9370±0.0500	3.800±0.100	90.000	4.222±0.111	0.464	0.0676±0.0297
^{203}Rn	^{199}Po	$(3/2^-)$	$(3/2^-)$	0	gs	gs	6.6298±0.0021	44.000±2.000	64.000	68.750±3.125		0.0442±0.0022
^{203}Rn^m		$(13/2^+)$	$(13/2^+)$	0	0.3620	0.3100	6.6818±0.0021	26.900±0.500	75.000	35.867±0.667	0.522	0.0523±0.0022
^{199}Fr	^{195}At	$[1/2^+]$	$1/2^+$	0	gs	gs	7.8100±0.0040	$(6.600\pm2.200)\times10^{-3}$	100	$(6.600\pm2.200)\times10^{-3}$		0.2269±0.0825
^{199}Fr^m		$[7/2^-]$	$(7/2^-)$	0	0.0047	0.0330	7.7817±0.0040	$(6.500\pm0.900)\times10^{-3}$	100	$(6.500\pm0.900)\times10^{-3}$	0.985	0.2580±0.0464
^{201}Fr	^{197}At	$(9/2^-)$	$(9/2^-)$	0	gs	gs	7.5160±0.0500	0.062±0.005	100	0.062±0.005		0.0873±0.0382
^{201}Fr^m		$(1/2^+)$	$(1/2^+)$	0	0.1290	0.0520	7.5930±0.0500	0.017±0.007	100	0.017±0.007	0.274	0.2356±0.1602
^{202}Fr	^{198}At	(3^+)	(3^+)	0	gs	gs	7.3890±0.0040	0.372±0.012	100	0.372±0.012		0.0808±0.0049
^{202}Fr^m		(10-)	(10-)	0	0.1020	0.1020	7.3890±0.0040	0.286±0.013	100	0.286±0.013	0.769	0.1052±0.0078
^{203}Fr	^{199}At	9/2-	(9/2-)	0	gs	gs	6.2600±0.0500	0.549±0.015	95.000	0.578±0.016		0.0204±0.0012
^{203}Fr^m		$(1/2^+)$	$1/2^+$	0	0.3610	0.2400	6.3810±0.0500	0.043±0.004	20.000	0.215±0.020	0.372	0.0555±0.0070
^{214}Fr	^{210}At	(1^-)	$(5)^+$	5	gs	gs	8.5890±0.0040	$(5.000\pm0.200)\times10^{-3}$	93.000	$(5.376\pm0.215)\times10^{-3}$		0.0050±0.0004
^{214}Fr		(1^-)	$(4)^+$	3	gs	0.0700	8.5190±0.0040	$(5.000\pm0.200)\times10^{-3}$	4.000	0.125±0.005		0.0001±0.00001
^{214}Fr^m		(8^-)	$(5)^+$	3	0.1220	gs	8.7110±0.0040	$(3.350\pm0.050)\times10^{-3}$	46.000	$(7.283\pm0.109)\times10^{-3}$	1.355	0.0003±0.00001
^{214}Fr^m		(8^-)	$(4)^+$	5	0.1220	0.0728	8.6382±0.0040	$(3.350\pm0.050)\times10^{-3}$	50.900	$(6.582\pm0.098)\times10^{-3}$	1.224	0.0029±0.0001
^{214}Fr^m	^{199}At	(8^-)	$(6)^+$	3	0.1220	0.5074	8.2036±0.0040	$(3.350\pm0.050)\times10^{-3}$	0.900	0.372±0.006	69.233	0.0009±0.00001

TABLE II. *(Continued).*

Pare.	Dau.	J_P^π	J_D^π	$l_{\min}$ ($\hbar$)	E_P (MeV)	E_D (MeV)	Q_α (MeV)	$T_{1/2}^{exp}$ (s)	I_α (%)	Γ_α^{exp} (s)	T_α/T_α^{min}(gs)	S_α^{exp} (Eq. (10))
^{215}Fr	^{211}At	$9/2^-$	$9/2^-$	0	gs	gs	9.5400±0.0070	$(8.600\pm0.500)\times10^{-8}$	100.000	$(8.600\pm0.500)\times10^{-8}$		0.0547 ± 0.0052
^{215}Fr^m		$(19/2)^-$	$9/2^-$	6	1.4400	gs	10.9800±0.0070	$(4.000\pm2.000)\times10^{-9}$	4.700	$(8.511\pm4.255)\times10^{-9}$	0.990	0.0036 ± 0.0019
^{215}Fr^n		$(23/2)^-$	$9/2^-$	8	1.5731	gs	11.1131±0.0070	$(3.500\pm1.400)\times10^{-9}$	4.100	$(8.537\pm3.415)\times10^{-9}$	0.993	0.0338 ± 0.0145
^{201}Ra	^{197}Rn	$(3/2^-)$	$(3/2^-)$	0	gs	gs	8.0020±0.0120	0.026±0.022	100	0.026±0.022		0.0501 ± 0.0436
^{201}Ra^m		$(13/2^+)$	$(13/2^+)$	0	0.2630	0.1990	8.0660±0.0120	0.006±0.005	100	0.006±0.005	0.231	0.1281 ± 0.1100
^{203}Ra	^{199}Rn	$(3/2^-)$	$(3/2^-)$	0	gs	gs	7.7300±0.0500	0.036±0.013	100	0.036±0.013		0.0897 ± 0.0571
^{203}Ra^m		$(13/2^+)$	$(13/2^+)$	0	0.2200	0.1800	7.7700±0.0500	0.025±0.005	100	0.025±0.005	0.694	0.1038 ± 0.0651
^{205}Ra	^{201}Rn	$(3/2^-)$	$(3/2^-)$	0	gs	gs	7.4860±0.0200	0.220±0.050	100	0.220±0.050		0.0679 ± 0.0251
^{205}Ra^m		$(13/2^+)$	$(13/2^+)$	0	0.2630	0.2450	7.5040±0.0200	0.180±0.050	100	0.180±0.050	0.818	0.0749 ± 0.0311
^{207}Ra	^{203}Rn	$(3/2^-)$	$3/2^-$	0	gs	gs	7.2700±0.0600	1.200±0.100	86.000	1.395±0.116		0.0685 ± 0.0361
^{207}Ra^m		$(13/2^+)$	$(13/2^+)$	0	0.5580	0.3620	7.4660±0.0600	0.059±0.004	15.000	0.393±0.027	0.282	0.0482 ± 0.0242
^{208}Ac	^{204}Fr	(3^+)	(3^+)	0	gs	gs	7.7300±0.0500	0.097±0.015	99.000	0.098±0.015		0.0558 ± 0.0277
^{208}Ac^m		(10^-)	(10^-)	0	0.5060	0.3160	7.9200±0.0500	0.028±0.007	90.000	0.031±0.008	0.318	0.0443 ± 0.0245
^{216}Th	^{212}Ra	0^+	0^+	0	gs	gs	8.0720±0.0040	$(2.600\pm0.020)\times10^{-2}$	99.600	$(2.610\pm0.020)\times10^{-2}$		0.0248 ± 0.0009
^{216}Th		0^+	2^+	2	gs	0.6293	7.4427±0.0040	$(2.600\pm0.020)\times10^{-2}$	0.400	6.500±0.050		0.0252 ± 0.0009
^{216}Th^m		(8^+)	0^+	8	2.0450	gs	10.1170±0.0040	$(1.330\pm0.040)\times10^{-4}$	2.100	$(6.333\pm0.191)\times10^{-3}$	0.243	0.0003 ± 0.00001
^{216}Th^m		(8^+)	2^+	6	2.0450	0.6293	9.4877±0.0040	$(1.330\pm0.040)\times10^{-4}$	0.360	$(3.694\pm0.111)\times10^{-2}$	1.415	0.0001 ± 0.00002
^{216}Th^m		(8^+)	8^+	0	2.0450	1.9670	8.1500±0.0040	$(1.330\pm0.040)\times10^{-4}$	0.360	$(3.694\pm0.111)\times10^{-2}$	1.415	0.0100 ± 0.0006
^{217}Pa	^{213}Ac	$9/2^-$	$9/2^-$	0	gs	gs	8.4890±0.0040	$(3.800\pm0.200)\times10^{-3}$	66.000	$(5.758\pm0.303)\times10^{-3}$		0.0151 ± 0.0012
^{217}Pa^m		$(23/2^-)$	$9/2^-$	8	1.8600	gs	10.3490±0.0040	$(1.080\pm0.030)\times10^{-3}$	53.000	$(2.038\pm0.057)\times10^{-4}$	0.354	0.0006 ± 0.0001
^{216}U	^{212}Th	0^+	0^+	0	gs	gs	8.5310±0.0260	$(6.900\pm2.900)\times10^{-3}$	100	$(6.900\pm2.900)\times10^{-3}$		0.0323 ± 0.0180
^{216}U^m		(8^+)	0^+	8	2.2400	gs	10.7710±0.0260	$(1.400\pm0.900)\times10^{-3}$	100	$(1.400\pm0.900)\times10^{-3}$	0.203	0.0001 ± 0.0001

TABLE III. Same as Table I, but for the translead nuclei that have isomers of less half-lives relative to their ground-state decays, $T_{1/2}(\text{isomer})/T_{1/2}(\text{gs}) < 0.1$.

Pare.	Dau.	J_P^π	J_D^π	$l_{\min}$ ($\hbar$)	E_P (MeV)	E_D (MeV)	Q_α (MeV)	$T_{1/2}^{exp}$ (s)	I_α (%)	T_α^{exp} (s)	T_α/T_α^{min}(gs)	S_α^{exp} (Eq. (10))
^{187}Bi	^{183}Tl	(9/2$^-$)	(1/2$^+$)	5	gs	gs	7.7790±0.0040	0.038±0.003	9.000	0.038±0.003		0.0005±0.0001
^{187}Bi		(9/2$^-$)	(9/2$^-$)	0	gs	0.6287	7.1503±0.0040	0.038±0.003	88.000	0.038±0.003		0.0676±0.0075
^{187}Bi^m		(1/2$^+$)	(1/2$^+$)	0	0.1120	gs	7.8910±0.0040	(3.700±0.200)×10^{-4}	100	(3.700±0.200)×10^{-4}	0.009	0.0308±0.0025
^{189}Bi	^{185}Tl	(9/2$^-$)	(1/2$^+$)	5	gs	gs	7.2700±0.0030	0.674±0.011	4.500	14.978±0.244		0.0015±0.0001
^{189}Bi		(9/2$^-$)	(9/2$^-$)	0	gs	0.4540	6.8160±0.0030	0.674±0.011	71.000	0.949±0.015		0.0450±0.0020
^{189}Bi^n		(1/2$^+$)	(1/2$^+$)	0	0.1850	gs	7.4550±0.0030	(5.000±0.400)×10^{-3}	73.000	(6.849±0.548)×10^{-3}	0.007	0.0349±0.0036
^{193}Bi	^{189}Tl	(9/2$^-$)	(1/2$^+$)	5	gs	gs	6.3070±0.0050	63.600±3.000	0.09	(7.067±0.333)×10^4		0.0009±0.0001
^{193}Bi		(9/2$^-$)	(9/2$^-$)	0	gs	0.2810	6.0260±0.0050	63.600±3.000	2.1	(3.029±0.143)×10^3		0.0221±0.0023
^{193}Bi^m		(1/2$^+$)	(1/2$^+$)	0	0.3080	gs	6.6150±0.0050	3.200±0.500	84	3.810±0.595	0.001	0.0557±0.0111
^{195}Bi	^{191}Tl	9/2$^{(-)}$	(1/2$^+$)	5	gs	gs	5.8320±0.0050	183.000±4.000	2.7×10^{-3}	(6.778±0.148)×10^6		0.0014±0.0001
^{195}Bi		9/2$^{(-)}$	9/2$^{(-)}$	0	gs	0.2990	5.5330±0.0050	183.000±4.000	0.027	(6.778±0.148)×10^5		0.0219±0.0018
^{195}Bi^m		(1/2$^+$)	(1/2$^+$)	0	0.3990	gs	6.2310±0.0050	87.000±1.000	33.000	263.636±3.030	4.0×10^{-4}	0.0266±0.0016
^{195}Bi^m		(1/2$^+$)	(3/2$^+$)	2	0.3990	0.3412	5.8898±0.0050	87.000±1.000	0.050	(1.740±0.020)×10^5	0.257	0.0028±0.0002
^{197}Bi	^{193}Tl	9/2$^{(-)}$	(9/2$^-$)	0	gs	0.3652	4.9998±0.0110	559.800±30.000	10^{-4}	(5.598±0.300)×10^8		0.0248±0.0051
^{197}Bi^m		(1/2$^+$)	1/2$^{(+)}$	0	0.5330	gs	5.8980±0.0110	309.000±33.000	60.000	515.000±55.000	9.2×10^{-7}	0.4169±0.0931
^{213}Ra	^{209}Rn	1/2$^-$	5/2$^-$	2	gs	gs	6.8613±0.0023	163.800±3.000	36.000	455.000±8.333		0.0083±0.0003
^{213}Ra		1/2$^-$	1/2$^-$	0	gs	0.1103	6.7510±0.0023	163.800±3.000	39.000	420.000±7.692		0.0138±0.0013
^{213}Ra		1/2$^-$	3/2$^-$	2	gs	0.2149	6.6464±0.0023	163.800±3.000	4.600	(3.561±0.065)×10^3		0.0080±0.0004
^{213}Ra^m		(17/2$^-$)	5/2$^-$	6	1.7700	gs	8.6313±0.0023	(2.180±0.040)×10^{-3}	0.600	0.363±0.007	0.001	0.0006±0.00001
^{213}Ra^m		(17/2$^-$)	1/2$^-$	8	1.7700	0.1101	8.5212±0.0023	(2.180±0.040)×10^{-3}	0.170	1.282±0.024	0.003	0.0036±0.0001
^{213}Ra^m		(17/2$^-$)	3/2$^-$	8	1.7700	0.2147	8.4166±0.0023	(2.180±0.040)×10^{-3}	0.021	10.380±0.191	0.025	0.0002±0.00001
^{214}Ra	^{210}Rn	0$^+$	0$^+$	0	gs	gs	7.2730±0.0030	2.460±0.030	99.780	2.465±0.030		0.0198±0.0007
^{214}Ra^n		8$^+$	0$^+$	8	1.8652	gs	9.1382±0.0030	(6.860±0.200)×10^{-5}	0.080	(8.575±0.250)×10^{-2}	0.035	0.0002±0.00001
^{214}Ra^n		8$^+$	8$^+$	0	1.8652	1.7090	7.4292±0.0030	(6.860±0.200)×10^{-5}	0.005	1.372±0.040	0.556	0.0067±0.0003

such as ^{216}Ac^{m} [9^{-} ($\pi 1h^{7}{}_{9/2^{-}} \bigotimes \nu 2g^{1}{}_{9/2^{+}}$), $T_{1/2}$(iso/gs) = 1.002], ^{214}Fr^{m} [8^{-} ($\pi 1h^{5}{}_{9/2^{-}} \bigotimes \nu 2g^{1}{}_{9/2^{+}}$), 0.670], and ^{212}At^{m} [9^{-} ($\pi 1h^{3}{}_{9/2^{-}} \bigotimes \nu 2g^{1}{}_{9/2^{+}}$), 0.379]. Additionally, there are relatively less stable isomers including ^{212}At^{n} (25^{-}), ^{214}Fr^{n} (11^{+}), and ^{214}Fr^{p} (33^{+}), all of which exhibit $T_{1/2}$(iso/gs) values less than 0.001. Similar phenomena are observed in isomers with paired protons, such as ^{217}Th^{n} [$25/2^{+}$, $T_{1/2}$(iso/gs) = 0.287], and the highly spin isomers of ^{211}Po^{n,p} ($31/2^{-}$, $43/2^{+}$), ^{213}Rn^{m,n,p} ($25/2^{+}$, $31/2^{-}$, $55/2^{+}$), ^{215}Rn^{m,n,p} ($25/2^{+}$, $29/2^{-}$, $43/2^{-}$), and ^{217}Th^{m} ($15/2^{-}$), all of which exhibit $T_{1/2}$(iso/gs) values ranging from 10^{-7} to 10^{-3}.

The presence of the unpaired valence eighty-fifth proton ($\pi 1h^{3}{}_{9/2^{-}}$) plays a significant role in the relatively higher stability of several isotopes, such as ^{192}At^{m} [(9^{-}, 10^{-} ($\pi 1h^{3}{}_{9/2^{-}} \bigotimes \nu 1i^{7}{}_{13/2^{+}}$)$T_{1/2}$(iso/gs) = 7.652], ^{191}At^{m} [$7/2^{-}$($\pi 1h^{3}{}_{9/2^{-}} \bigotimes \nu 1i^{6}{}_{13/2^{+}}$), 1.048], ^{194}At^{m} [9^{-}, 10^{-} ($\pi 1h^{3}{}_{9/2^{-}} \bigotimes \nu 1i^{9}{}_{13/2^{+}}$), 1.129], and ^{214}At^{n} [9^{-} ($\pi 1h^{3}{}_{9/2^{-}} \bigotimes \nu 2g^{3}{}_{9/2^{+}}$), 1.362]. This proton couples with the single $\nu 1i^{7}{}_{13/2^{+}}$, $\nu 1i^{9}{}_{13/2^{+}}$, and $\nu 2g^{3}{}_{9/2^{+}}$ neutrons in ^{192}At^{m}, ^{194}At^{m}, and ^{214}At^{n}, respectively. The coupling between the valence proton $\pi 1h^{3}{}_{9/2^{-}}$ ($\pi 2f^{1}{}_{7/2^{-}}$ [69]) and the $\nu 2g^{3}{}_{9/2^{+}}$ neutron results in the observation of negative-parity states ranging from 0^{-} to 9^{-} for ^{214}At, except 5^{-} state, within a narrow energy range. Furthermore, the $1/2^{+}$ state is observed as a stable isomeric state in ^{197}At^{m} [($1/2^{+}$, $T_{1/2}$(iso/gs) = 5.249], as well as the less stable isomers ^{199}At^{m} ($1/2^{+}$, 0.045) and ^{201}At^{m} ($1/2^{+}$, 0.0005), and as the ground states of ^{191,193,195}At, and the low-lying state of ^{201,203}At. This can be attributed to a ($\pi 1h^{4}{}_{9/2^{-}} \bigotimes 3s^{-1}{}_{1/2^{+}}$) proton configuration rather than $\pi 1h^{3}{}_{9/2^{-}}$, as explained earlier for the odd-A Bi^{m}($1/2^{+}$) isomers. Additionally, the observation of ^{193}At^{n} ($13/2^{+}$, 0.966), ^{197}At^{m} ($13/2^{+}$, 10^{-6}), ^{199}At^{n} ($13/2^{+}$, 10^{-8}), ^{193}At^{m} ($7/2^{-}$, 0.724), and ^{195}At^{m} ($7/2^{-}$, 0.493) suggests the promotion of the unpaired proton in the $\pi 1h^{3}{}_{9/2^{-}}$ orbital to the vacant $\pi 1i_{13/2^{+}}$ ($\pi 2f_{7/2^{-}}$) orbitals. The coupling between the valence proton state ($\pi 1h^{3}{}_{9/2^{-}}$, $\pi 1i^{1}{}_{13/2^{+}}$, or $\pi 2f^{1}{}_{7/2^{-}}$) and the valence neutron state ($\nu 3p^{1}{}_{3/2^{-}}$ or $\nu 1i_{13/2^{+}}$) leads to the presence of various isomers such as ^{200}At^{m} [7^{+}, $T_{1/2}$(iso/gs) = 1.093], ^{202}At^{m} (7^{+}, 0.989), ^{216}At^{m} (9^{-}, 0.333), ^{198}At^{m} (7^{+}, 0.280), ^{200}At^{n} (10^{-}, 0.081), and ^{202}At^{n} (10^{-}, 0.003), as well as the relatively less stable isomers ^{196}At^{m,n}(5^{+}, 10^{-}) and ^{204,206}At^{m}(10^{-}). In addition to the observation of the relatively more stable ^{213}At^{n}[$49/2^{+}$ ($\pi 1h^{3}{}_{9/2^{-}} \bigotimes \nu 2g^{2}{}_{9/2^{+}}$), $T_{1/2}$(iso/gs) = 360], other high-spin At (even-N) isomers with less relative stability have been observed, namely ^{199,201,205,209}At^{m,n,p} ($29/2^{+}$), ^{207}At^{m} ($25/2^{+}$), ^{211}At^{m} ($39/2^{-}$), as well as ^{208}At^{m} (16^{-}), ^{210}At^{m,n} (15^{-}, 19^{+}), and ^{212}At^{n} (25^{-}), which exhibit both unpaired neutron and unpaired proton configurations.

The coupling of the unpaired eighty-seventh proton in the $\pi 1h^{5}{}_{9/2^{-}}$ orbital with an unpaired neutron contributes to the stability of the observed isomers ^{218}Fr^{m} [8^{-}, 9^{-} ($\pi 1h^{5}{}_{9/2^{-}} \bigotimes \nu 2g^{5}{}_{9/2^{+}}$), $T_{1/2}$(iso/gs) = 21.900], ^{200}Fr^{m} [10^{-} ($\pi 1h^{5}{}_{9/2^{-}} \bigotimes \nu 1i^{13}{}_{13/2^{+}}$), 3.878], ^{216}Fr^{m} [9^{-} ($\pi 1h^{5}{}_{9/2^{-}} \bigotimes \nu 2g^{3}{}_{9/2^{+}}$), 1.214], ^{204}Fr^{m} [7^{+} ($\pi 1h^{5}{}_{9/2^{-}} \bigotimes \nu 3p^{3}{}_{3/2^{-}}$), 1.053], and ^{206}Fr^{m} [7^{+} ($\pi 1h^{5}{}_{9/2^{-}} \bigotimes \nu 2f^{1}{}_{5/2^{-}}$), 1.000], which show longer or comparable half-lives relative to their ground states. The coupling between the valence $\pi 1h^{5}{}_{9/2^{-}}$ proton and another valence neutron also appears in the isomers ^{202,204,208}Fr^{m,n}(10^{-}), ^{216}Fr^{n}(3^{-}), and ^{212,214}Fr^{m,n} (11^{+}), which are less stable than their ground states. Additionally, the valence $\pi 1h^{5}{}_{9/2^{-}}$ proton promotes to another orbital in the isomers ^{199}Fr^{m}($7/2^{-}$) and ^{201,203,205}Fr^{m,n}($1/2^{+}$, $13/2^{+}$), which exhibit $T_{1/2}$(iso/gs) values less than 1. Within the excitation energy range up to 3.068 MeV, ^{215}Fr exhibits multiple stable states with half-lives of nanoseconds, with spins of $9/2^{-}$(gs), $13/2^{+}$, $17/2^{-}$, $15/2^{-}$, $19/2^{-}$, $23/2^{-}$, $27/2^{-}$, $29/2^{+}$, $33/2^{+}$, $33/2^{-}$, and $39/2^{-}$ [64]. Furthermore, other high-spin Fr isomers with relatively lower stability have been also observed, such as ^{212}Fr^{n,p}(15^{-}, 27^{-}), ^{209}Fr^{m}($45/2^{-}$), ^{211}Fr^{m,n}($29/2^{+}$, $45/2^{-}$), and ^{213}Fr^{m,n}($21/2^{-}$, $29/2^{+}$), as well as the highest-spin isomers ^{214}Fr^{p}(33^{+}) and ^{213}Fr^{p}($65/2^{-}$). For instance, the $29/2^{+}$ state of the odd-A Fr isomers can be attributed to the $\pi 1h^{4}{}_{9/2} \bigotimes i_{13/2}$ configuration, with a single proton in the $1i_{13/2}$ orbital and coupling of two protons in $1h_{9/2}$ orbital to spin eight [69], with a typical ground-state configuration of paired neutrons.

The obtained values of spectroscopic preformation factor S_{α}^{expt} that indicates the α-preformation probability ranges from 0.0003 [^{218}Fr^{m}(9^{-})] to 0.417 [^{197}Bi^{m}($1/2^{+}$)], with an average value of 0.068, for the favored decays of all investigated isomers. Less values within the range from 0.0006 [^{210}Bi(1^{-})] to 0.227 [^{199}Fr($1/2^{+}$)], with an average value of 0.051, are obtained for the corresponding decays of the same nuclei in their ground states. The isomeric states then indicate larger α-preformation probability than ground states. For the investigated unfavored decays, S_{α}^{expt} lies between 10^{-11} [^{210}Bi^{m}(9^{-})$\rightarrow$ ^{206}Tl(1^{-}), $l_{\min} = 10$] and 0.129 [^{212}Po^{m}(8^{-})], with an average value of 0.006, for the isomeric states, and between 10^{-5} [^{214}Fr(1^{-})] and 0.025 [^{216}Th(0^{+})], with an average value of 0.006, for the nuclei in ground states. While the maximum transferred angular momentum of the unfavored decay modes of the investigated isomers is $l_{\min} = 11$ [^{217}Ac^{m} ($29/2^{+}$)$\rightarrow$ ^{213}Fr ($9/2^{-}$, $7/2^{-}$)], that of nuclei in ground-states is five, which lowers the indicated preformation probability inside isomers for unfavored decays. Figure 3(a) displays the estimated preformation probability for the different decay modes of Bi isotopes, in their ground and isomeric states, as function of the energy of the parent Bi state. The obtained values of S_{α} presented in Tables I, II and III, and in Fig. 3(a), indicated that the favored decays from the isomeric states yield larger preformation probability than ground states. The unfavored decay modes from the isomeric states indicate the smallest preformation probabilities, due to the higher values of the transferred angular momentum by the emitted α particle in such decays.

The favored decays from the investigated isomers can be classified into two categories, namely, the decays in which the isomeric state is of higher energy than the state of the daughter nucleus (32 decays) and decays from lower- to higher-energy state (28 decays). While the former decays ($E_P \geqslant E_D$) yield preformation probability within the range

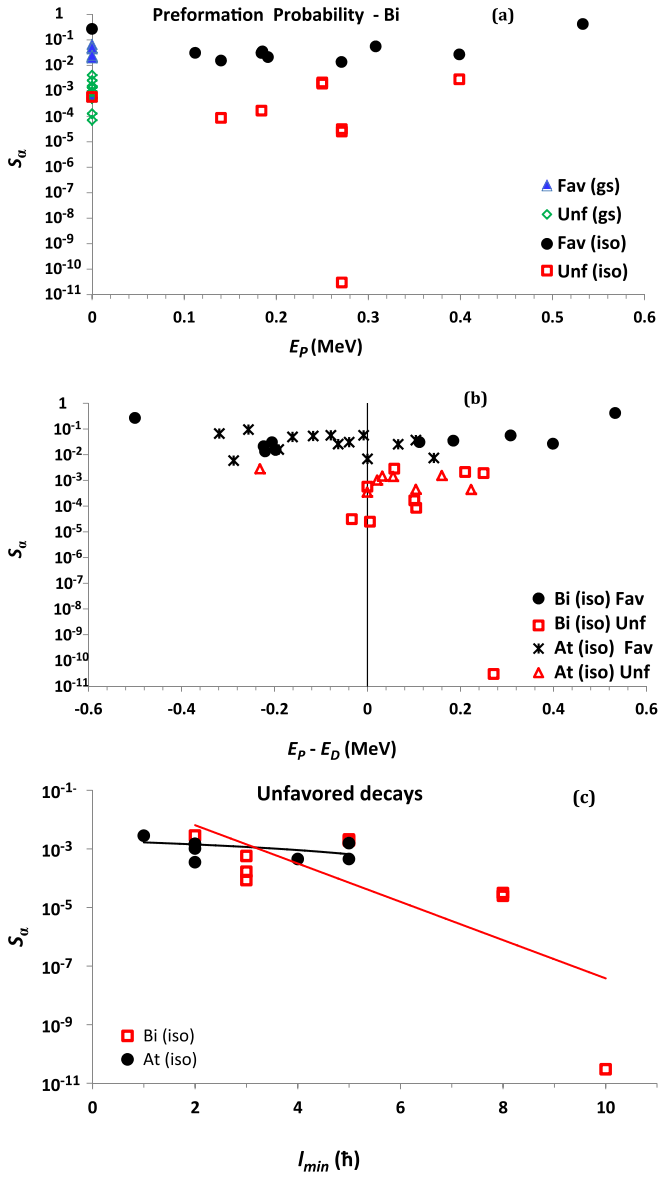

FIG. 3. The preformation probability S_α^{expt} as extracted from the T_α^{expt} and T_α^{calc} (without S_α) for (a) the decay modes of Bi isotopes, in ground and isomeric states, against the energy of the parent state, and for (b) the favored and unfavored decay modes of Bi and At isomers, against the difference in energy between parent and daughter energy states. (c) S_α^{expt} for the unfavored decays of Bi and At isomers, versus the minimum transfer of the orbital angular momentum, carried by the emitted α particle, according to the conservation of angular momentum.

from 0.007 to 0.417, the latter ($E_P < E_D$) indicate lower-values range from 10^{-4} to 0.287. On the contrary, the former exhibit lower-values range of T_α(iso/gs) range, from 10^{-6} to 4.2, than the latter that shows a range from 0.02 to 418. The corresponding favored decays from the ground states of the same nuclei yield a range of S_α from 0.005 to 0.227. The favored ground-state decays corresponding to fifteen of the investigated isomeric states with $E_P < E_D$ take place to excited states of daughter nuclei. Such ground-state decays indicate preformation probability range from 0.001 to 0.154. The isomers of excitation energy lower than their daughter nuclei then indicate less preformation probability and larger T_α(iso/gs) values than the isomers of higher excitation energy than their daughters.

On the other hand, the unfavored decays from the studied isomers can be divided into four sets, namely, the decays of $E_P \geqslant E_D$ without (24 decays) or with (12) a change in parity, and those of $E_P < E_D$ without (7) or with (2) parity change. These decay types yield an average (maximum) preformation probability of about 0.0090 (0.1285), 0.0012 (0.0046), 0.0020 (0.0041), and 0.0019 (0.0028), respectively, taking into consideration that the last type appears only in two decay modes. Excluding the extreme large value of T_α(iso/gs) $= 10^8$ of the decay mode [^{210}Bi$^m(9^-) \rightarrow$ ^{206}Tl(1^-)], the corresponding average values of T_α(iso/gs) for the same sets are about 1439, 1028, 569, and 69, respectively. The larger preformation probability for the unfavored decays of isomers appears then for those keep the parity unchanged. All the isomers of $T_{1/2}$(iso/gs) < 0.001 decay to daughter states of less energy, and the unfavored decays among them do not change parity. One of the key factors influencing both the preformation probability and the half-life against a given decay mode is the orbital angular momentum l_α carried by the emitted α particle. Figure 3(b) displays the extracted preformation probability for favored and unfavored decay modes of the Bi and At isomers, as a function of the difference in energy ($E_P - E_D$) between the parent and daughter states among them the decay modes take places. The same quantity is displayed in Fig. 3(c) for the unfavored decays of Bi and At isomers, as a function of the minimum angular momentum l_{min} allowed for the emitted α particle. As seen in Fig. 3(b), the estimated preformation probability tends to increase with increasing the difference of energy, $E_P - E_D$. Increasing the minimum required value of angular momentum indicates less preformation probability, as clearly seen in Fig. 3(c). This is why many isomers of high spin exhibit more relative stability than their ground states, either generally or against certain decay modes, as described above for ^{210}Bi$^m(9^-)$ and ^{211}Po$^m(25/2^+)$.

IV. SUMMARY AND CONCLUSIONS

The most appearing isomers among the observed 292 translead isomers from ^{187}Pb$(13/2^+)$ to ^{239}U$(5/2^+)$ are those of Bi and Pb, which contribute with 57 and 55 isomers, respectively. The most appearing isotones are those of $N = 126$ (24 isomers) and $N = 127$ (19 isomers). ^{210}Bi^m $(9^-,\ T_{1/2} = 3.04$ My), ^{204}Pb^n $(9^-,\ 67.93$ min), and ^{201}Bi^m $(1/2^+,\ 57.50$ min) are the most stable translead isomers. ^{210}Bi^m [$(9^-,\ T_{1/2}$(iso/gs) $= 2.2 \times 10^8$] is also the most stable isomer relative to its ground state, then ^{213}At^n $(49/2^+,\ 360)$ and ^{211}Po^m $(49/2^+,\ 48.8)$. The highest-spin appear for the ^{214}Fr^p (33^+), ^{213}Fr^p $(65/2^-)$, and ^{211}Rn^n $(63/2^-)$ isomers. The isotones of $N = 126 \pm 1$ contribute about 60% of the observed isomers of high spin $\geqslant 17\hbar$. We have used the relative values of the total $T_{1/2}$(iso/gs) and α decay T_α(iso/gs) half-life of the isomer relative to its ground-state half-life, to scrutinize the factors that merely influence the stability of the isomeric state, far away that determine the absolute stability of the nucleus. Both the single valence $Z = 83$ proton and $N = 127$

neutron, outside the doubly magic Pb core, were indicated to play a main role in enhancing the stability of the translead isomers, either they remain in their original $\pi 1h^1{}_{9/2^-}$ and $\nu 2g^1{}_{9/2^+}$ orbitals or when they promote to another orbital. The promotion or coupling of the unpaired valence 85th ($\pi 1h^3{}_{9/2^-}$) and 87th ($\pi 1h^5{}_{9/2^-}$) protons similarly contribute to the relatively stable At and Fr isomers, respectively. The presence of an unpaired neutron is found to increase the stability of the isomer, relative to its corresponding ground-state nucleus, either when it leaves its original orbital to another one or when it couples with a single valence proton. In many cases, a proton (neutron) pair may decouple with promotion of one of them to a vacancy in other orbital, leaving excited state with a hole. The high-spin of spin-gap isomers can be attributed to stretching two protons (neutrons) to have large spin, which couples in turn with a single valence proton (neutron).

We investigated 105 α-decay modes of 70 isomers from ^{187}Pb$(13/2^+)$ to ^{218}U(8^+), and compared them with their corresponding ground-state decays. $\log_{10} T_\alpha$ of the different α decay of isomers, as well as of their corresponding ground states, are found to increase linearly with $(Q_\alpha^{-1})^{1/2}$, yielding distinguishable characteristic lines for the different values of $l_{\min}$, which would help to estimate unknown spin-parity assignments. Increasing l_α of a given decay mode increases its corresponding half-life. For the favored decay modes, the isomeric states tend to indicate larger α-preformation probability than their corresponding ground states. The favored decay modes from higher isomeric state to lower energy state of daughter nuclei indicate larger S_α and lower T_α(iso/gs) than those from lower to higher-energy states. The key factors influencing both the preformation probability and the half-life against a given decay mode are the orbital angular momentum needed to be carried by the emitted α particle and the parity of the involved states. Larger values of l_α appear in the decays of isomers to low-lying energy states of daughter nuclei, which indicate less preformation probability in isomers for unfavored decays. This is the reason why many isomers of high spin are relatively more stable than their corresponding ground states. Moreover, the unfavored decays involving a change in parity from the parent to daughter nuclei exhibit less preformation probability relative to those keep the parity unchanged. Increasing the difference in energy between the parent and daughter states tend to indicate larger preformation probability. The smallest T_α(iso/gs) for the unfavored decays of isomers are indicated for those from lower E_P to higher E_D energy state of opposite parity. Understanding such correlations between nuclear structure and the stability of isomers builds a basis towards the optimal benefit of nuclear isomers as a form of energy storage.

[1] W. M. Seif and A. S. Hashem, J. Phys. G **47**, 085103 (2020).
[2] W. M. Seif, G. G. Adamian, N. V. Antonenko, and A. S. Hashem, Phys. Rev. C **104**, 014317 (2021).
[3] M. Ismail, W. M. Seif, and W. M. Tawfik, Indian J. Phys. **96**, 875 (2022).
[4] W. M. Seif, A. R. Abdulghany, and A. Nasr, Int. J. Mod. Phys. E **31**, 2250074 (2022).
[5] J. G. Deng and H. F. Zhang, Phys. Lett. B **816**, 136247 (2021).
[6] Y. Z. Wang, J. M. Dong, B. B. Peng, and H. F. Zhang, Phys. Rev. C **81**, 067301 (2010).
[7] K. Yoshida and J. Tanaka, Phys. Rev. C **106**, 014621 (2022).
[8] M. Asai, F. P. Heßberger, and A. Lopez-Martens, Nucl. Phys. A **944**, 308 (2015).
[9] A. I. Budaca and I. Silisteanu, J. Phys.: Conf. Ser. **413**, 012027 (2013).
[10] D. Ni, Z. Ren, T. Dong, and Y. Qian, Phys. Rev. C **87**, 024310 (2013).
[11] W. M. Seif, N. V. Antonenko, G. G. Adamian, and H. Anwer, Phys. Rev. C **96**, 054328 (2017).
[12] M. Ismail, W. M. Seif, A. Adel, and A. Abdurrahman, Nucl. Phys. A **958**, 202 (2017).
[13] D. Ni and Z. Ren, Phys. Rev. C **93**, 054318 (2016).
[14] Y. Qian and Z. Ren, Nucl. Phys. A **945**, 134 (2016).
[15] W. M. Seif, Phys. Rev. C **74**, 034302 (2006).
[16] W. M. Seif, M. Shalaby, and M. F. Alrakshy, Phys. Rev. C **84**, 064608 (2011).
[17] W. M. Seif and A. S. Hashem, Chin. Phys. C **42**, 064104 (2018).
[18] W. Ye, Y. Qian, and Z. Ren, Phys. Rev. C **104**, 064308 (2021).
[19] F. Soddy, Nature (London) **99**, 244 (1917).
[20] O. Hahn, Chem. Ber. **54**, 1131 (1921).
[21] B. Seiferle, L. von der Wense, and P. G. Thirolf, Phys. Rev. Lett. **118**, 042501 (2017).
[22] J. J. Carroll, Laser Phys. Lett. **1**, 275 (2004).
[23] G. W. Misch, S. K. Ghorui, P. Banerjee, Y. Sun, and M. R. Mumpower, Astrophys. J., Suppl. Ser. **252**, 2 (2020).
[24] R. D. Herzberg, P. T. Greenlees, P. A. Butler, G. D. Jones, M. Venhart, I. G. Darby, and J. Uusitalo, Nature (London) **442**, 896 (2006).
[25] S. Stellmer, G. Kazakov, M. Schreitl, H. Kaser, M. Kolbe, and T. Schumm, Phys. Rev. A **97**, 062506 (2018).
[26] M. Pospelov, S. Rajendran, and H. Ramani, Phys. Rev. D **101**, 055001 (2020).
[27] F. G. Kondev, M. Wang, W. J. Huang, S. Naimi, and G. Audi, Chin. Phys. C **45**, 030001 (2021).
[28] S. Garg, B. Maheshwari, B. Singh, Y. Sun, A. Goel, and A. K. Jain, At. Data Nucl. Data Tables **150**, 101546 (2023).
[29] G. Lotay, A. Lennarz, C. Ruiz, C. Akers, A. A. Chen, G. Christian, and A. S. J. Murphy, Phys. Rev. Lett. **128**, 042701 (2022).
[30] P. M. Walker and Z. Podolyak, *Handbook of Nuclear Physics* (Springer Nature, Singapore, 2022), pp. 1–37.
[31] P. M. Walker, Nucl. Phys. A **834**, 22c (2010).
[32] E. V. Tkalya, Phys. Rev. Lett. **106**, 162501 (2011).
[33] L. A. Rivlin, Quantum Electron. **37**, 723 (2007).
[34] J. J. Liu *et al.*, Phys. Rev. C **102**, 024301 (2020).
[35] W. M. Seif, M. Ismail, and E. T. Zeini, J. Phys. G **44**, 055102 (2017).
[36] J.-G. Deng, J.-C. Zhao, D. Xiang, and X.-H. Li, Phys. Rev. C **96**, 024318 (2017).
[37] P. Walker and G. Dracoulis, Nature (London) **399**, 35 (1999).
[38] A. K. Jain, B. Maheshwari, A. Goel, A. K. Jain, B. Maheshwari, and A. Goel, Nuclear Isomers: A Primer (Springer Nature, Switzerland, 2021), pp. 17–33.

[39] A. N. Andreyev, M. Kowalska, S. Naimi, K. Blaum, S. Kreim, M. Breitenfeldt, and F. Herfurth, CERN-INTC-2011-009 (2011).
[40] P. M. Walker and G. D. Dracoulis, Hyperfine Interact. **135**, 83 (2001).
[41] P. M. Walker, Phys. Scr. **92**, 054001 (2017).
[42] S. G. Wahid, S. K. Tandel, S. Suman, P. C. Srivastava, A. Kumar, P. Chowdhury, and S. Zhu, Phys. Lett. B **832**, 137262 (2022).
[43] K. E. Karakatsanis, G. A. Lalazissis, V. Prassa, and P. Ring, Phys. Rev. C **102**, 034311 (2020).
[44] M. R. Mumpower, P. Jaffke, M. Verriere, and J. Randrup, Phys. Rev. C **101**, 054607 (2020).
[45] V. Rakopoulos, M. Lantz, S. Pomp, A. Solders, A. Al-Adili, L. Canete, T. Eronen, A. Jokinen, A. Kankainen, A. Mattera, I. D. Moore, D. A. Nesterenko, M. Reponen, S. Rinta-Antila, A. deRoubin, M. Vilen, M. Osterlund, H. Penttilä, Phys. Rev. C **99**, 014617 (2019).
[46] K. Yadav, A. Y. Deo, P. C. Srivastava, S. K. Tandel, S. G. Wahid, S. Kumar, and A. K. Jain, Phys. Rev. C **105**, 034307 (2022).
[47] M. Iriondo, D. Jerrestam, and R. J. Liotta, Nucl. Phys. A **454**, 252 (1986).
[48] S. S. Malik and R. K. Gupta, Phys. Rev. C **39**, 1992 (1989).
[49] B. Buck, A. C. Merchant, and S. M. Perez, Phys. Rev. C **45**, 2247 (1992).
[50] W. M. Seif, J. Phys. G **40**, 105102 (2013).
[51] J. W. Negele and D. Vautherin, Phys. Rev. C **5**, 1472 (1972).
[52] C. Titin-Schnaider and Ph. Quentin, Phys. Lett. B **49**, 213 (1974).
[53] M. J. Giannoni and P. Quentin, Phys. Rev. C **21**, 2076 (1980).
[54] E. Chabanat, E. Bonche, E. Haensel, J. Meyer, and R. Schaeffer, Nucl. Phys. A **635**, 231 (1998).
[55] P. Möller, A. J. Sierk, T. Ichikawa, and H. Sagawa, At. Data Nucl. Data Tables **109-110**, 1 (2016).
[56] W. M. Seif and H. Mansour, Int. J. Mod. Phys. E **24**, 1550083 (2015).
[57] P.-G. Reinhard, *Computational Nuclear Physics*, edited by K. Langanke, J. A. Maruhn, S. E. Koonin (Springer-Verlag, Berlin, 1990), Vol. 1, p. 28.
[58] W. M. Seif and A. Adel, Phys. Rev. C **99**, 044311 (2019).
[59] N. G. Kelkar, H. M. Castañeda, and M. Nowakowski, Europhys. Lett. **85**, 20006 (2009).
[60] W. M. Seif and A. Abdurrahman, Chin. Phys. C **42**, 014106 (2018).
[61] W. M. Seif, M. Ismail, A. I. Refaie, and L. H. Amer, J. Phys. G **43**, 075101 (2016).
[62] D. N. Poenaru and R. A. Gherghescu, J. Phys. G **41**, 125104 (2014)
[63] R. A. Gherghescu, W. Greiner, and D. N. Poenaru, Phys. Rev. C **52**, 2636 (1995).
[64] National Nuclear Data Center (NNDC), Brookhaven National Laboratory, http://www.nndc.bnl.gov.
[65] G. Audi, F. G. Kondev, Meng Wang, W. J. Huang, and S. Naimi, Chin. Phys. C **41**, 030001 (2017).
[66] M. Wang, G. Audi, F. G. Kondev, W. J. Huang, S. Naimi, and X. Xu, Chin. Phys. C **41**, 030003 (2017).
[67] P. K. Hopke, R. A. Naumann, and K. H. Sejewski, Phys. Rev. **187**, 1709 (1969).
[68] K. Yanase, E. Teruya, K. Higashiyama, and N. Yoshinaga, Phys. Rev. C **98**, 014308 (2018).
[69] E. Teruya, K. Higashiyama, and N. Yoshinaga, Phys. Rev. C **93**, 064327 (2016).